APOE4 drives inflammation in human astrocytes via TAGLN3 repression and NF-κB activation

Laurie Arnaud, Philippe Benech, Louise Greetham, Delphine Stephan, Angélique Jimenez, Nicolas Jullien, Laura García-González, Philipp Tsvetkov, François Devred, Ignacio Sancho-Martinez, et al.

Cell Reports

Article

APOE4 drives inflammation in human astrocytes via TAGLN3 repression and NF-κB activation

Graphical abstract

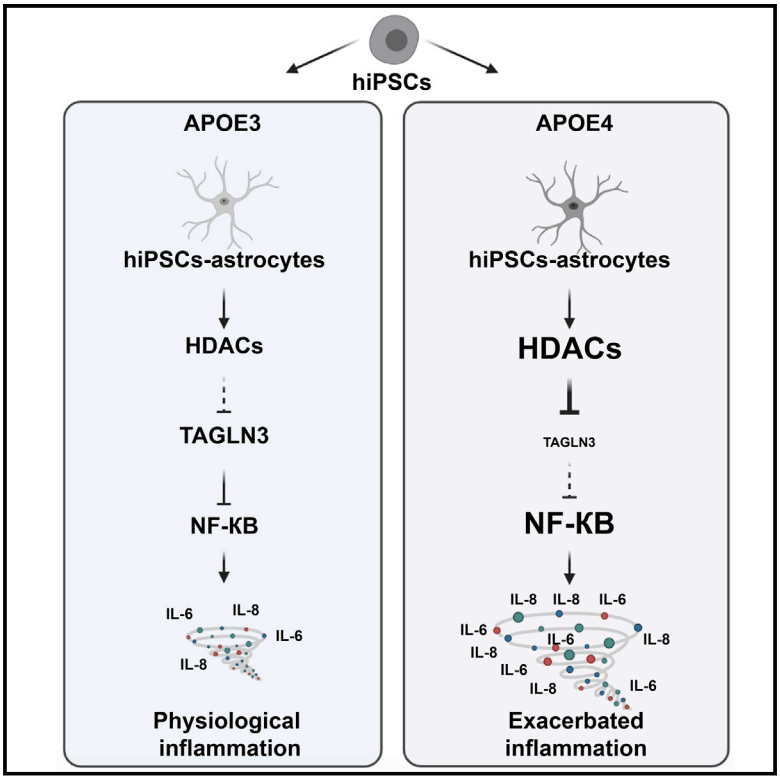

Highlights

- hiPSC astrocytes carrying the *APOE*ε4 allele feature a pro-inflammatory phenotype
- APOE4 associates with TAGLN3 downregulation and NF-κB activation in astrocytes
- TAGLN3 supplementation in APOE4 astrocytes reduces inflammatory responses
- TAGLN3 downregulation is a common trait in brains from patients with Alzheimer's disease

Authors

Laurie Arnaud, Philippe Benech, Louise Greetham, ..., Kévin Baranger, Santiago Rivera, Emmanuel Nivet

Correspondence

emmanuel.nivet@univ-amu.fr

In brief

Arnaud et al. show that human astrocytes carrying the main genetic risk for Alzheimer's disease, namely APOE4, are more prone to inflammation. They identify TAGLN3 downregulation in astrocytes as a mechanism underlying inflammatory dysfunctions in APOE4 carriers. Therefore, they highlight TAGLN3 as a target of interest for anti-neuroinflammatory strategies.

Arnaud et al., 2022, Cell Reports *40*, 111200
August 16, 2022
https://doi.org/10.1016/j.celrep.2022.111200

CellPress

Cell Reports

CellPress
OPEN ACCESS

Article

APOE4 drives inflammation in human astrocytes via TAGLN3 repression and NF-κB activation

Laurie Arnaud,[1] Philippe Benech,[1] Louise Greetham,[1] Delphine Stephan,[1] Angélique Jimenez,[1] Nicolas Jullien,[1] Laura García-González,[1] Philipp O. Tsvetkov,[1] François Devred,[1] Ignacio Sancho-Martinez,[2] Juan Carlos Izpisua Belmonte,[3] Kévin Baranger,[1,4] Santiago Rivera,[1] and Emmanuel Nivet[1,5,*]

[1]Aix-Marseille Univ, CNRS, INP, Inst Neurophysiopathol, Marseille, France
[2]FAES Farma, Leioa 48940, Spain
[3]Altos Labs, Inc., 5510 Morehouse Drive, Suite 300, San Diego, CA 92121, USA
[4]Present address: UMRi CNRS 7266 LIENSs, BCBS group (Biotechnologies et Chimie des Bioressources pour la Santé), La Rochelle University, 17000 La Rochelle, France
[5]Lead contact
*Correspondence: emmanuel.nivet@univ-amu.fr
https://doi.org/10.1016/j.celrep.2022.111200

SUMMARY

Apolipoprotein E4 (*APOEε4*) is the major allelic risk factor for late-onset sporadic Alzheimer's disease (sAD). Inflammation is increasingly considered as critical in sAD initiation and progression. Identifying brain molecular mechanisms that could bridge these two risk factors remain unelucidated. Leveraging induced pluripotent stem cell (iPSC)-based strategies, we demonstrate that APOE controls inflammation in human astrocytes by regulating Transgelin 3 (TAGLN3) expression and, ultimately, nuclear factor κB (NF-κB) activation. We uncover that APOE4 specifically downregulates TAGLN3, involving histone deacetylases activity, which results in low-grade chronic inflammation and hyperactivated inflammatory responses. We show that APOE4 exerts a dominant negative effect to prime astrocytes toward a pro-inflammatory state that is pharmacologically reversible by TAGLN3 supplementation. We further confirm that TAGLN3 is downregulated in the brain of patients with sAD. Our findings highlight the APOE-TAGLN3-NF-κB axis regulating neuroinflammation in human astrocytes and reveal TAGLN3 as a molecular target to modulate neuroinflammation, as well as a potential biomarker for AD.

INTRODUCTION

Apolipoprotein E (APOE) is primarily known as a key regulator of lipid homeostasis, and, within the brain, it plays a critical role in cholesterol and phospholipids transport to neurons. APOE exists in three main isoforms in human (APOE2, APOE3, APOE4), with astrocytes being the main source in the brain (Pitas et al., 1987). The *APOEε4* allele is by far the major genetic variant linked to sporadic Alzheimer's disease (sAD) (Corder et al., 1993; Kunkle et al., 2019). APOE4 has been previously involved in beta amyloid (Aβ) plaque formation (Liu et al., 2017; Huang et al., 2017), tau-mediated neurodegeneration (Shi et al., 2017; Wang et al., 2021), and blood-brain-barrier breakdown (Montagne et al., 2021), three of the major hallmarks of AD. Chronic neuroinflammation is another key feature in AD, and the *APOEε4* allele was found to correlate with reactive gliosis in the AD brain (Zhu et al., 2012). Overall, a large body of evidence has progressively unveiled pleiotropic functions for APOE that are linked to AD pathology (Huang and Mahley, 2014), including in inflammation (Yin et al., 2019; Rodriguez et al., 2014; Shi and Holtzman, 2018). Indeed, studies have shown a cross-talk between APOE and inflammatory mediators such as cytokines (Zhang et al., 2011), revealing an intricate APOE-mediated regulation of inflammatory and immune responses. Along this line, a recent study has revealed that the *APOEε4* allele primes microglial cells toward a pro-inflammatory state in normal aging as well as in AD (Serrano-Pozo et al., 2021). However, despite progresses, the mechanisms by which APOE variants may affect the control of inflammation in the brain are scarce (Yin et al., 2019). More specifically, the precise role of APOE4 in astrocytes and its mechanistic connection to pathological neuroinflammation remain unclear. Thus, identifying mechanisms underlying early astrocytic inflammatory dysfunctions in *APOEε4* carriers may unveil pathogenic molecular events that might shed lights on the critical role of changes in brain immune competence and their link to AD initiation/progression.

Neuroinflammatory changes are among the earliest brain manifestations in AD (Schöll et al., 2015), even before the onset of Aβ accumulation, and are increasingly considered as critical in pathogenesis initiation and progression (Dominy et al., 2019; Kinney et al., 2018). Further supported by converging genetic data linking an increased AD risk to inflammatory-related genes, neuroinflammation has therefore emerged as one of the possible drivers supporting plaque formation in the brain of patients with AD (Blasko et al., 1999; Sutinen et al., 2012). Moreover, a recent study has demonstrated a role for microglial nuclear factor κB

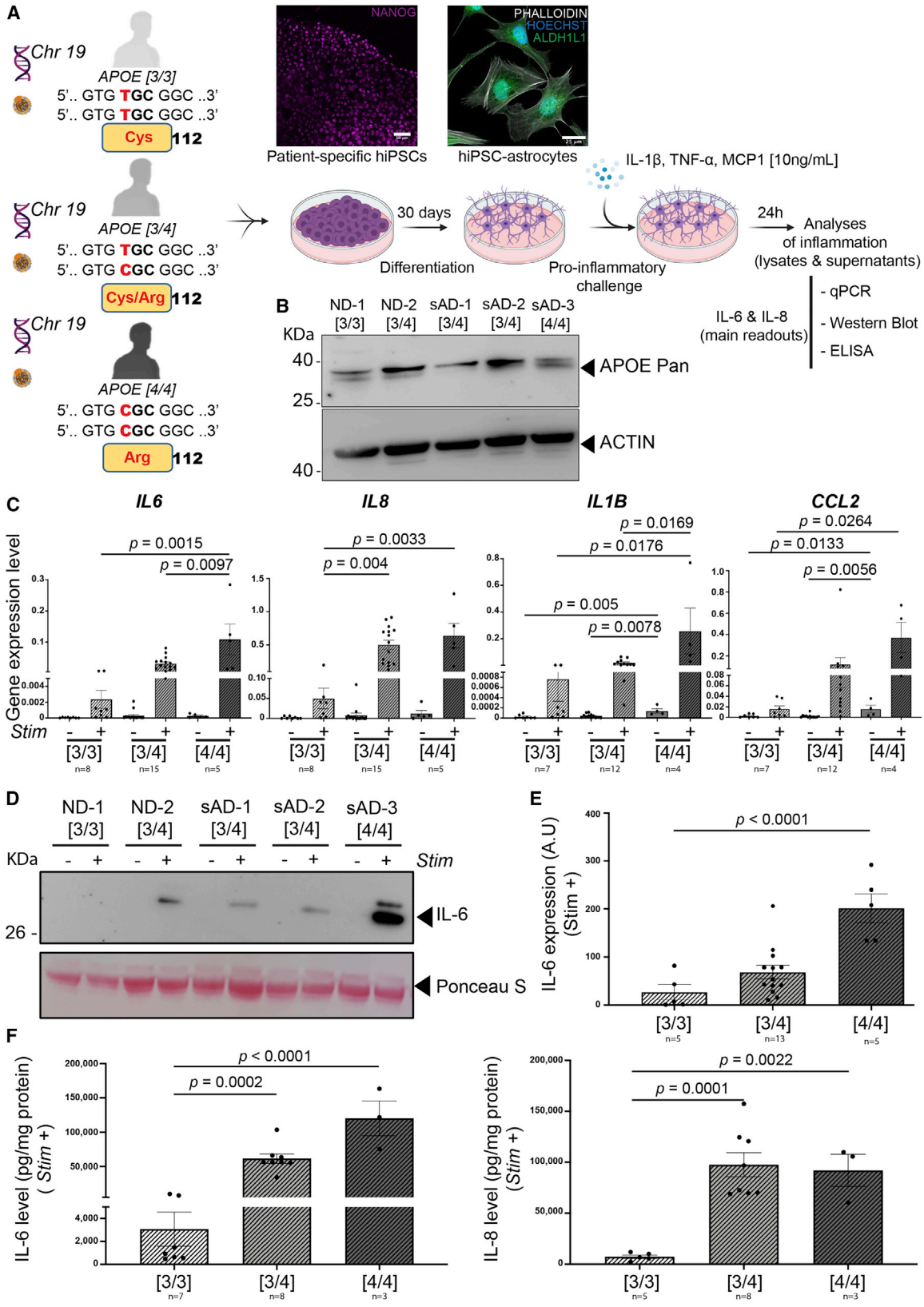

(legend on next page)

(NF-κB) signaling in mediating tau spreading and toxicity in tauopathy (Wang et al., 2022). Beside genetic factors, aging is the main risk factor in AD, and immune changes brought on by age advancement such as immunosenescence and inflammaging are linked to AD pathology (Martorana et al., 2012). Yet, the mechanisms of pathogenic inflammation in the brain remain largely unknown. Consequently, identifying the early drivers of altered brain immune responses remain an urgent research need, owing to the potential to identify therapeutic targets. To do so, however, the prevailing neuron-centric view in AD, based on the dominant amyloid hypothesis (Selkoe and Hardy, 2016), has to be shifted to one that also considers the contribution of glial cells, the major cell contributors to neuroinflammation. Astrocytes are numerous and are, functionally, an important glial cell type in the brain but were long neglected in neurodegenerative studies, though they have gained increased interest (Arranz and De Strooper, 2019; Wang et al., 2021). Astrocytes provide homeostatic control to the brain (Verkhratsky and Nedergaard, 2018), support neuronal functions, maintain blood-brain-barrier integrity, and also regulate innate and adaptive immune responses in the central nervous system (CNS) (Giovannoni and Quintana, 2020). Morphology changes in astrocytes have long been observed in the context of neurodegenerative diseases and linked to inflammatory responses (Sofroniew and Vinters, 2010). Moreover, the critical role of reactive astrocytes in AD and their relevance as cell targets for therapeutic intervention were demonstrated in AD mouse models (Ceyzériat et al., 2018; Furman et al., 2012). Therefore, mechanistic understanding on the astrocytic pathways controlling inflammation might be of critical interest to intervene therapeutically in AD.

Given the differences between human and rodent astrocytes (Zhang et al., 2016), it is becoming urgent to get a more comprehensive understanding on how APOE4 could affect inflammatory responses from human astrocytes. Patient-specific induced pluripotent stem cells (iPSCs) with AD-linked polymorphisms at risk for AD, together with gene-editing techniques, offer promising models for studying disease pathogenesis in relevant cell types, including human astrocytes (Lin et al., 2018). Leveraging these technologies, we found that APOE4 iPSC-derived astrocytes exhibit a higher basal expression of inflammation-related genes and an enhanced inducibility in response to cytokines when compared with their APOE3 counterparts. We found that APOE4 causes negative dominance on APOE3 to establish a pro-inflammatory disease phenotype in human astrocytes. Furthermore, we identified the APOE-TAGLN3-NF-κB axis that is dysregulated in astrocytes from patients with AD carrying the *APOE*ε4 allele. Indeed, in APOE4 astrocytes, we found that TAGLN3 downregulation exacerbates inflammation through NF-κB activation, which led us to identify TAGLN3 as an interacting partner of IκBα. Further investigations demonstrate that such a downregulation is under the control of APOE4-dependent histone deacetylase (HDAC) activity. We showed that pharmacological interventions at different levels of this regulatory axis of the brain immune system, including TAGLN3 supplementation, can rescue the disease phenotype observed in astrocytes. We next confirmed that TAGLN3 was downregulated in the brain of *APOE*ε4 carriers but also found similar results in the brain of patients with non-*APOE*ε4 sAD. The description of this altered neuroinflammatory regulatory axis suggests TAGLN3 as a lead candidate to prevent the risk for AD-like brain damages caused by inflammatory dysfunctions.

RESULTS

*APOE*ε4 carriers display a pro-inflammatory phenotype in patient-specific hiPSC-astrocytes

To first determine whether carrying the *APOE*ε4 allele can affect inflammatory-associated functions in human astrocytes, we used multiple human iPSC (hiPSC) lines derived from patients with sAD and non-demented (ND) controls. Human iPSC lines presenting different *APOE* genotypes, including [*APOE3/E3*], [*APOE3/E4*], and [*APOE4/E4*] (Figures 1A, S1A, and S1B; Table S1), were differentiated into neural progenitor derivatives prior to generating astrocyte-like cells (Tcw et al., 2017) (Figure 1A). Successful differentiation and high purity of cultures was validated by the expression of a set of astrocytic markers (*GLAST*, *GFAP*, *VIMENTIN*, *AQUA4*, *CD44*), along with the absence of cells expressing the neuronal markers *NEUN* and *TUJ1* (Figures 1A, S1C, and S1D). Importantly, immunoblotting analysis revealed that hiPSC astrocytes produce the APOE (Figure 1B). Differentiated astrocytes were then challenged with a cocktail of pro-inflammatory cytokines (interleukin-1β [IL-1β], MCP-1 and tumor necrosis factor alpha [TNF-α]), representative of microglia-secreted inflammatory mediators in AD (Wang et al., 2015) (Figure 1A). Demonstrating

Figure 1. hiPSC-derived APOE4 astrocytes display an exacerbated inflammation

hiPSCs from a non-demented (ND) control donor and patients with sporadic Alzheimer's disease (sAD), carrying different *APOE* polymorphisms [*APOE3/E3*] ([3/3], n = 1), [*APOE3/E4*] ([3/4], n = 3), and [*APOE4/E4*] ([4/4], n = 1), were differentiated into astrocytes prior to challenging with a pro-inflammatory cocktail (IL-1β, MCP-1, and TNF-α). Twenty-four h after the stimulus (*Stim*), cell lysates and supernatants were analyzed for inflammatory mediators.

(A) Scheme depicting the experimental paradigm. Top inserts show immunostainings against the NANOG pluripotency marker (purple, top left) and ALDH1L1-positive astrocytes (green, top right) counterstained with the actin filaments marker PHALLOIDIN (white) and the Hoechst blue nuclei marker (blue).

(B) Western blot validating the APOE expression (lysates) in patient-specific hiPSC astrocytes. ACTIN was used as loading control.

(C) Quantification of *IL6*, *IL8*, *IL1B*, and *CCL2* mRNA levels, using qPCR analyses, from multiple patient-specific astrocytes.

(D) Representative western blots for IL-6 production (supernatants) from patient-specific astrocyte cultures. Ponceau staining was used as loading control.

(E) Secreted levels of IL-6, quantified by relative intensities, from western blot analyses.

(F) Absolute quantification of secreted IL-6 and IL-8 by ELISA.

(C–F) In all assays, one [3/3], three [3/4], and one [4/4] lines were analyzed, with 2–8 independent batches of differentiation for each line. The "n" under each genotype/experimental condition indicates the total number of independent batches of differentiation analyzed and pooled. Data are presented as mean ± SEM using one-way ANOVA followed by post hoc Tukey's test (C) or Dunnett's test (E and F). In (E), A.U. stands for arbitrary units (see STAR Methods). Scale bars: (A), 50 (top left insert) and 25 μm (top right insert).

For additional data and controls, see also Figure S1.

responsiveness to this cytokine-based cocktail, and thus astrocyte activation, a gene-expression profile highlighted the upregulation of all four pre-selected and key pro-inflammatory mediators we chose to analyze, namely *IL6*, *IL8*, *IL1B*, and *CCL2* (Figure 1C). Most interestingly, our data highlighted significantly higher levels of these genes in an APOE4-dependent manner (Figure 1C). Of importance, IL-6 and the IL-8 (not included in our cocktail) have been linked to the AD pathology in humans (Hull et al., 1996; Hu et al., 2019), which led us to mainly focus our analyses on these two pro-inflammatory mediators for the rest of our study. Western blotting and ELISA on IL-6 and IL-8 further confirmed their upregulation at the protein level (Figures 1D–1F). As per RNA analyses, upregulated protein levels were directly correlated to APOE4, following a rank potency order of [*APOE4/E4*] > [*APOE3/E4*] > [*APOE3/E3*] (Figures 1D–1F). Of note, for several of the analyzed inflammatory mediators, APOE4 astrocytes demonstrated higher basal cytokine levels when compared with APOE3 astrocytes (Figure 1C). Of note, [*APOE4/E3*] astrocytes derived from an ND control individual showed cytokine levels similar to those obtained from patients with sAD (Figure S1E). These results suggested that the differential efficacy in the inflammatory response was dependent on APOE and not influenced by the AD status. Further supporting these observations, [*APOE3/E3*] astrocytes from a patient with sAD showed an overall reduced inflammatory response compared with sAD *APOE4* carriers (Figure S1E). Altogether, this suggests a central role for APOE in modulating inflammation in human astrocytes.

*APOE*ε4 knockin and APOE knockout drive a pro-inflammatory phenotype in human astrocytes

When using patient-specific iPSCs as a modeling strategy to study the specific action of a given protein in human cell derivatives, one must consider the possibility that the genetic diversity from each individual could bring confounding factors on a given process. Therefore, to unequivocally investigate the role of APOE in controlling astrocytic inflammatory responses, we leverage the power of CRISPR technologies. We generated [*APOE4/E4*] knockin (KI) and APOE knockout (KO) isogenic clones (n = 3 clones/line) from [*APOE3/E3*] hiPSCs derived from an ND donor and from a patient with sAD (Figures 2A and S2). Sanger sequencing analyses confirmed the absence of mutation in predicted off-target sites (Table S2). We confirmed that the karyotypes of the edited [*APOE4/E4*]-KI clones were normal (Figure S2E). The edited lines maintained the typical hallmarks of iPSCs as confirmed by the expression of pluripotency markers in [*APOE4/E4*]-KI lines (Figure S2F). As before, isogenic [*APOE4/E4*]-KI astrocytes demonstrated increased cytokine levels at both RNA and protein levels in either unstimulated or stimulated conditions when compared with the control (Figures 2B, S3A, and S3C). This reinforced the notion that APOE3 controls inflammation in astrocytes and indicated that the presence of the *APOE*ε4 allele leads to chronic inflammation. Of further interest, we observed similar results from isogenic APOE-KO astrocytes, also displaying significantly higher basal release of pro-inflammatory mediators and greater responses upon stimulation, as measured by IL-6 and IL-8 levels (Figures 2B, S3A, and S3C). These data indicate that the effects observed in APOE4 astrocytes could be the result, at least in part, of a loss of homeostatic function. Importantly, our results were highly reproducible between three independent genome-edited clones. This ruled out possible off-target effects but also the possibility that the pro-inflammatory phenotype we observed in patient-specific astrocytes was the result of a reminiscent disease state prior to reprogramming. Of note, similar results were obtained from the [*APOE3/E3*] sAD line and its isogenic APOE4 and APOE-KO genome-edited clones, as demonstrated by significantly higher IL-8 levels (Figure S3D). Together, these data position APOE as a core regulator of inflammation in human astrocytes and demonstrate that APOE4 confers a higher susceptibility to inflammation.

APOE4 acts through a dominant negative effect to dysregulate inflammation in astrocytes

Our analyses in patient-specific astrocytes revealed that APOE4 homozygotes display greater inflammatory responses than APOE4 heterozygotes (Figures 1C–1F). This suggested that the presence of APOE3 together with APOE4 in astrocytes could reduce, but not fully rescue, the pro-inflammatory effect of APOE4 alone. Accordingly, we sought to determine whether exogenous APOE3 could modulate the inflammatory response from [*APOE4/E4*] astrocytes. First, cytokine-stimulated [*APOE4/E4*] astrocytes were co-treated with an [*APOE3/E3*] astrocyte conditioned medium prepared for either 72 or 168 h. Twenty-four h after co-treatment, we could not detect a significant reduction of the inflammatory responses from APOE4/E4 astrocytes (Figure S3E). We thought that this may be explained by the low levels of secreted APOE3 found in the conditioned media at 1.28 and 3.06 ng/mL after 72 and 168 h, respectively, as measured by ELISA, which led us to use higher doses of APOE3 as a recombinant protein in the next series of experiments. Addition of recombinant APOE3 to the culture significantly reduced the release of both IL-6 and IL-8 from [*APOE4/E4*] astrocytes upon stimulation (Figures 2C and 2D). The uptake of exogenous APOE3 by astrocytes upon supplementation in the serum-containing culture media was confirmed in a dose-dependent manner (Figure 2C). Inversely, incubation of [*APOE3/E3*] astrocytes with human APOE4 recombinant protein led to an exacerbated inflammatory response upon stimulation (Figures 2E and 2F). Whereas APOE3 supplementation showed a dose-response anti-inflammatory effect in the tested range of concentrations—i.e., from 15 to 120 μg/mL—the strong pro-inflammatory effect of APOE4 was immediate and reached a plateau from the first tested dose (i.e., 15 μg/mL). In line with our previous observations highlighting the role of the endogenous APOE independently of an AD background, these experiments further demonstrate the direct regulation of inflammation by APOE3 and the exacerbated pro-inflammatory responses obtained in the presence of the APOE4 isoform. Implicit in these results is that APOE4 may act through a dominant negative effect. To test this, we first identified that exogenous application of APOE3 at high dosage (400 μg/mL) could significantly rescue the loss of homeostatic function that was observed in the absence of endogenous APOE, i.e., in APOE-KO astrocytes (Figure 3A). Next, we applied a mixture of both APOE4 and APOE3, at different concentration ratios, in APOE-KO astrocytes. We observed that applying a 1:40 dose ratio of a mixture of APOE4 and APOE3 could start recapitulating the pro-inflammatory phenotype observed in APOE4 astrocytes as

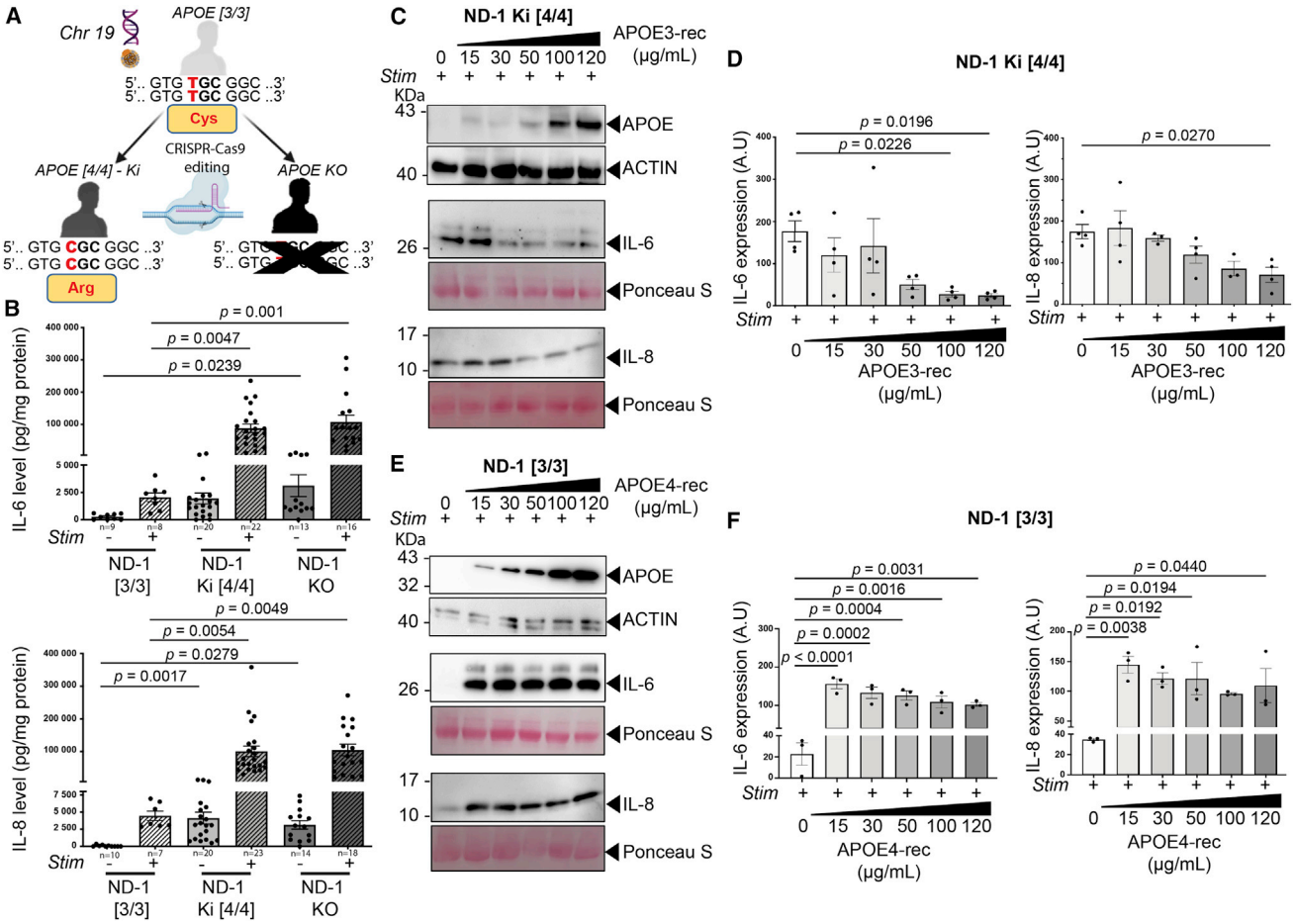

Figure 2. CRISPR-Cas9 editing and pharmacological interventions reveal an APOE-dependent control of inflammation in human astrocytes

(A) Scheme depicting the experimental paradigm to generate isogenic controls, allowing the generation of [*APOE4/E4*]-knockin (KI) and *APOE*-knockout (KO) hiPSCs from [*APOE3/E3*] hiPSC lines.

(B) Quantification by ELISA of the levels of IL-6 and IL-8 in the supernatants of astrocyte cultures from an ND donor (ND-1 [3/3], n = 1) and its respective independent KI (ND-1 Ki [4/4], n = 3 independent lines) and KO (ND-1 KO, n = 3 independent lines) isogenic control lines, with 4–10 independent batches of differentiation for each line. The "n" under each genotype/experimental condition indicates the total number of independent batches of differentiation analyzed and pooled.

(C–F) Upon application of a pro-inflammatory Stim, APOE3 and APOE4 as recombinant proteins (APOE3-and APOE4-rec), were respectively applied on [*APOE4/E4*]-KI (n = 3, independent lines) or [*APOE3/E3*] astrocytes (n = 1 line). Dose-response analyses were performed.

(C and D) Representative western blots (C) and quantification (D) of IL-6 and IL-8 from APOE3-rec-treated [*APOE4/E4*]-KI astrocytes (n = 4/dose, with 1 or 2 independent batches of differentiation/line).

(E and F) Representative western blots (E) and quantification (F) of IL-6 and IL-8 from APOE4-rec-treated [*APOE3/E3*] astrocytes (n = 3/dose, with 3 independent batches of differentiation).

Data are presented as mean ± SEM using one-way ANOVA followed by post hoc Dunnett's test (B, D, and F). In (D) and (F), A.U. stands for arbitrary units (see STAR Methods).

For additional data and controls, see also Figures S2 and S3.

shown by an increase of IL-6 and IL-8 levels (Figure 3B). We observed that this pro-inflammatory effect was further exacerbated and significant at a 1:4 ratio (Figure 3B). Altogether, our data demonstrate that APOE4 loses the regulatory function of inflammation ascribed to APOE3 but also interferes with this function in heterozygous cells.

We next tested whether this dominant negative effect of APOE4 could be due to its change of structure. To that end, [*APOE4/E4*] astrocytes were incubated with the PH-002 compound, a well-characterized APOE4-structure corrector that converts APOE4 into an APOE3-like molecule (Chen et al., 2012). We observed that PH-002 strikingly reduced the pro-inflammatory phenotype displayed by [*APOE4/E4*] astrocytes (Figures 3C–3E). These data showed that APOE3 finely tunes the inflammatory response from human astrocytes and that the conformational change in APOE4 deregulates a control system that is otherwise safeguarded by APOE3.

APOE4 enhances basal expression of cytokine target genes toward higher NF-κB activity

Next, we sought to investigate the mechanisms by which APOE regulates inflammation in human astrocytes by identifying genes

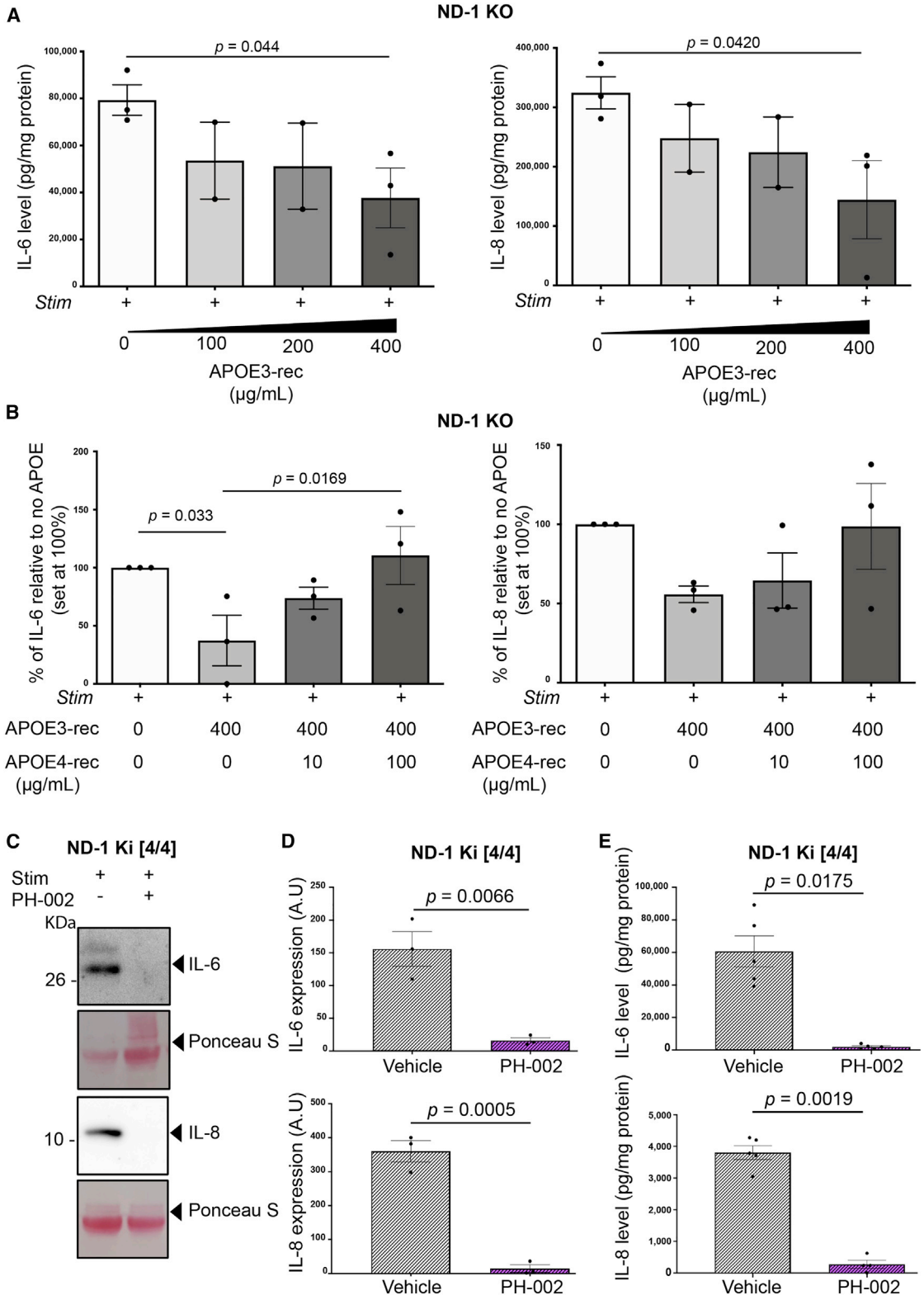

Figure 3. Structure-dependent dominant negative effect of APOE4 on inflammation

(A) APOE-KO astrocytes (n = 2 or 3 independent lines) were co-treated with a pro-inflammatory cocktail (Stim) along with increasing concentrations of APOE3 as recombinant protein (n = 3/dose, with 1 batch of differentiation/line). Twenty-four h later, the secreted levels of IL-6 and IL-8 were measured by ELISA.

(legend continued on next page)

exhibiting differential expression between [*APOE4/E4*] and [*APOE3/E3*]. To this end, we used our experimental paradigm in isogenic hiPSC astrocytes to evaluate gene-expression changes that were induced by the sole T > C substitution converting *APOE3* into *APOE4*. At first, we found 1,441 genes exhibiting a higher basal expression in [*APOE4/E4*] astrocytes than in [*APOE3/E3*] astrocytes (Figure 4A). Among them, 286 (33%) were found to be induced by our pro-inflammatory cocktail in [*APOE3/E3*] astrocytes and 85 (23%) in stimulated [*APOE4/E4*] astrocytes, while 272 genes (32% of the stimulated [*APOE3/E3*] and 76% of the simulated [*APOE4/E4*] astrocytes) were common to both genotypes. Pathway analysis revealed an enrichment for genes involved in cell cycle, cell division, the regulation of the cell-cycle process, cytokine signaling in immune system, and cellular responses to stress amongst the top 5 pathways found overrepresented in [APOE4/E4]-KI astrocytes (Figure S4A). Interestingly, a significant number of genes eliciting a higher basal expression in [*APOE4/E4*] astrocytes was known to be cytokine-targeted genes such as *CCL2*, *CXCL1*, *CXCL2*, *CXCL5*, *CXCL6*, *LIF*, *LY6E*, *MX1*, and *WARS* (Table S3). In addition, we observed that genes such as *REL*, *RELB*, *NFKB1*, *NFKB2*, and *NFKBIA,* all encoding several components of the NF-κB pathway, were significantly upregulated in [*APOE4/E4*] astrocytes (Table S3). Altogether, these data suggested that APOE4 enhances inflammation via an increase of NF-κB activity. Moreover, we noticed that 158 genes induced in both [*APOE3/E3*] and isogenic [*APOE4/E4*] astrocytes exhibited no difference in their basal expression. This set of genes included several known cytokine-induced genes such as *C1QTNF1*, *CCL20*, *CCL5*, *CSF2*, *CXCL8*, *IDO1*, *LOXL2*, *MMP10*, *OASL*, *PTGS2*, *SP100*, *STAT1*, *IFI6*, *MX2*, and *IRF7*, suggesting their regulation toward a mechanism independent of APOE.

These results prompted us to specifically analyze the effect of the APOE genotype on the NF-κB signaling pathway. Protein analyses on different NF-κB members, those found overexpressed in [*APOE4/E4*] astrocytes, showed an overall tendency to be higher in [*APOE4/E4*] astrocytes, thus confirming gene-expression data (Figures 4B and 4C). Indeed, nearly all the NF-κB members we analyzed were found to be significantly increased in APOE-KO astrocytes compared with APOE3/E3 in non-stimulated conditions, whereas there were no significant differences between APOE-KO and APOE4/E4 astrocytes. Importantly, significantly higher levels of phosphorylated IκBα, the latter being the inhibitory regulator of NF-κB when non-phosphorylated, were also observed in [*APOE4/E4*] and APOE-KO astrocytes (Figures 4B and 4C). This further suggests a constitutive hyperactive NF-κB pathway in *APOE4*-carrying astrocytes, possibly due to a loss of homeostatic function. The levels of p50 and p100, members of the canonical and non-canonical pathways, respectively, were significantly increased in APOE-KO astrocytes (Figures 4B and 4C). Seemingly, the levels of p52, the active derivative of p100, were also significantly increased in both [*APOE4/E4*] and APOE-KO astrocytes (Figures 4B and 4C). Nuclear fractionation experiments confirmed increased nuclear translocation for p50 and p52 in [*APOE4/E4*] astrocytes, which is known to trigger NF-κB activation (Figures S4B and S4C). Immunostainings against p65 further confirmed these observations and revealed an overall higher nuclear translocation of p65, including in its phosphorylated form, in [*APOE4/E4*] astrocytes (Figures 4D and S4D). Taken together, our data highlight that activation of the NF-κB signaling pathway is a key driver of APOE-mediated inflammatory responses.

APOE4 downregulates TAGLN3 to drive a pro-inflammatory signature in human astrocytes via NF-κB activation

We next used a text-mining-based software (Patatian and Benech, 2020) to investigate the correlations between APOE, inflammation, and the genes differentially expressed in [*APOE4/E4*] astrocytes, which could provide further insights on the molecular mechanisms altered by APOE4. This approach led us to identify a correlation with the reduced expression of *Transgelin 3 (TAGLN3*) in [*APOE4/E4*] astrocytes, a gene encoding the TAGLN3 protein that is almost exclusively expressed in the CNS (Ito et al., 2005). We focused our attention on TAGLN3 since previous reports have associated an increase in inflammation with reduced expression of its close homolog SM22a/TAGLN1 in APOE-null vascular smooth muscle cells (VSMCs) (Dai et al., 2017; Shen et al., 2010). At the protein level, we confirmed that TAGLN3 was readily detected in APOE3 astrocytes while barely expressed in both [*APOE4/E4*] and APOE-KO isogenic astrocytes (Figures 5A, 5B, and S5A). Addition of exogenous APOE3 to [*APOE4/E4*] astrocytes restored TAGLN3 levels in a dose-dependent manner (Figures 5C and 5D) and was accompanied by a remarkable decrease of the IL-6 levels (Figure 5C), the latter confirming our observations (Figures 2C and 2D). Similar effects were observed with the PH-002 APOE4 structural corrector, which significantly induced TAGLN3 expression in [*APOE4/E4*] astrocytes (Figures 5E and 5F) accompanied by reduced levels of p50 and p52 (Figures 5G and 5H). Of note, since no previous data have ever been reported regarding TAGLN3 expression in astrocytes, we investigated the localization of this protein after cell fractionation. TAGLN3 was mainly detected in the cytosol and the nucleus of hiPSC astrocytes

(B) APOE-KO astrocytes (n = 2 or 3 independent lines) were co-treated with a pro-inflammatory cocktail (Stim) along with a mixture of both APOE4 and APOE3 (as recombinant protein), at different concentration ratios as indicated (n = 3/condition, with 1 batch of differentiation/line). Twenty-four h later, for each of the three tested isogenic clones, the secreted levels of IL-6 and IL-8 were measured by ELISA and compared with their respective control condition, i.e., no APOE treatment. Data are expressed as a percentage of the control condition.

(C and D) Along with their stimulation with a pro-inflammatory cocktail (Stim), [*APOE4/E4*]-KI astrocytes (n = 3 independent lines) were treated with an APOE4-structure corrector (PH-002, 100 μM) or its control vehicle. Representative western blots (C) and quantification (D) of IL-6 and IL-8 from PH-002-treated [*APOE4/E4*]-KI astrocytes (n = 3/condition, with 1 batch of differentiation/line).

(E) Quantification of the levels of IL-6 and IL-8 in the supernatants of [*APOE4/E4*]-Ki astrocytes (n = 3 independent lines) treated with PH-002 24 h prior to stimulation, as measured by ELISA (n = 5/condition, with 1–2 batches of differentiation/line).

Data are presented as mean ± SEM using unpaired two-tailed Student's t test (D and E) or using one-way ANOVA followed by post hoc Fisher's least significant difference (LSD) test (A and B). In (D), A.U. stands for arbitrary units (see STAR Methods).

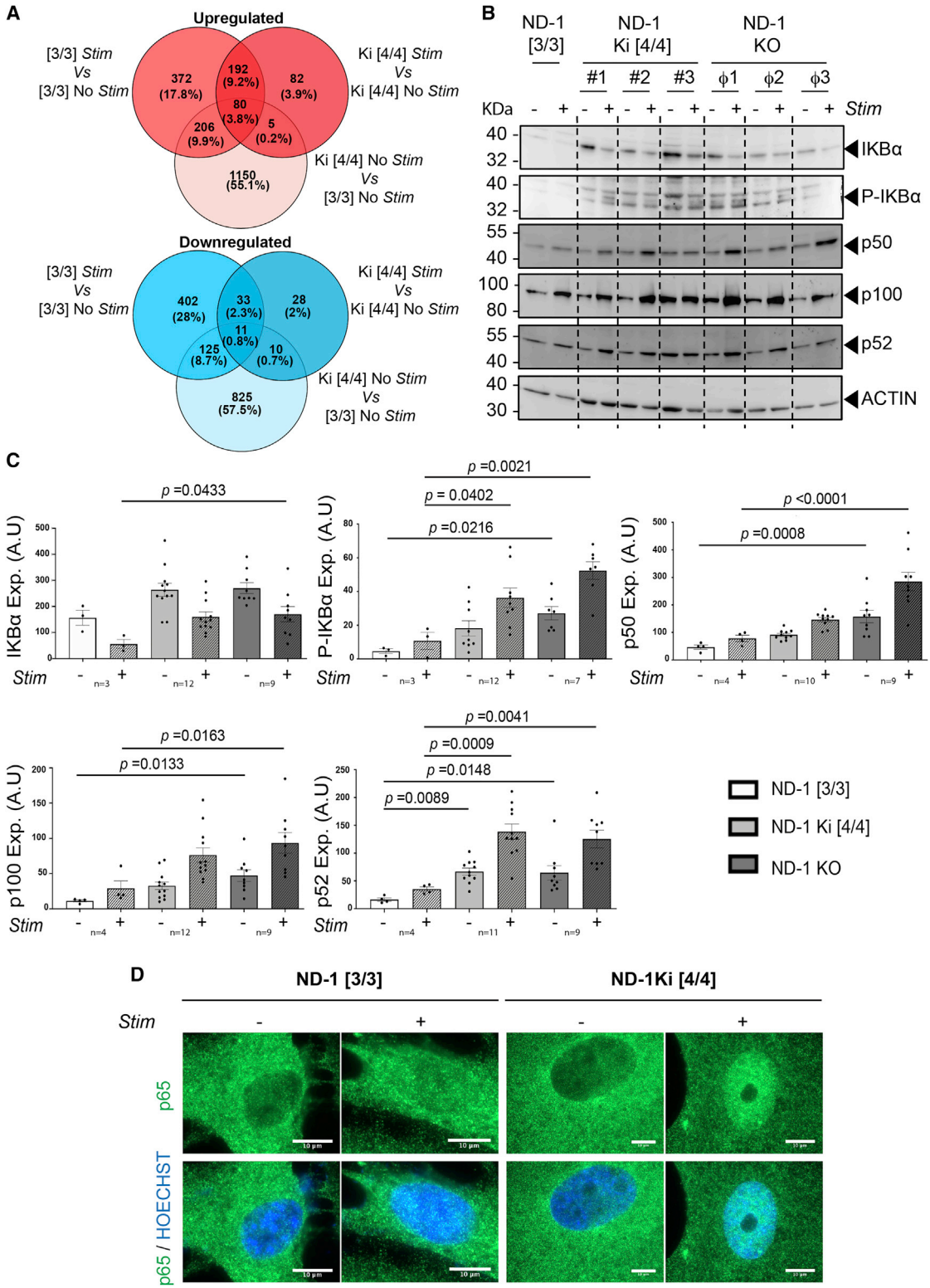

Figure 4. APOE4-dependent pro-inflammation involves NF-κB activity

(A) Venn diagrams depicting the distribution of upregulated (red circles, top) and downregulated (blue circles, bottom) genes according to their differential expression between [*APOE3/E3*] (n = 1) and their [*APOE4/E4*]-KI isogenic astrocytes (n = 3 independent lines), either in unstimulated (no stim) or stimulated (Stim) conditions. Fold change (FC) cut-offs used for analyses were ≥1.5 and ≤0.6 for 975 upregulated and downregulated genes, respectively.

(legend continued on next page)

but not in the cytoskeleton and was barely detectable at the membrane (Figure S5B). Altogether, these data demonstrated, within human astrocytes, the existence of intracellular mechanistic connections between APOE, the regulation of TAGLN3, and NF-κB activity.

We next conducted rescue experiments to investigate whether this APOE-TAGLN3 axis was responsible for controlling inflammation in human astrocytes. Exogenous application of TAGLN3 reduced the inflammatory response of [*APOE4/E4*] astrocytes (Figures 6A and S5C–S5E). Of importance, intracellular levels of TAGLN3 were found concomitantly rescued in the treated cells (Figures S5C and S5D), thus demonstrating that exogenous TAGLN3 can be internalized by astrocytes. This was also concomitant with a significant lower expression of p50 and p52 subunits in a dose-dependent manner, ultimately demonstrating that TAGLN3 controls the NF-κB pathway in human astrocytes (Figures 6B and 6C). Further supporting that TAGLN3 negatively regulates inflammation in astrocytes, the stimulation of APOE3 astrocytes also led to TAGLN3 downregulation (Figure 6D). The latter suggested that pro-inflammatory responses from astrocytes involve the removal of TAGLN3-associated inhibition on the NF-κB activity. These data demonstrate TAGLN3 repression as a molecular mechanism underlying neuroinflammation in astrocytes.

Next, we asked whether TAGLN3 regulation of NF-κB activity could be mediated, at least partly, through IκBα, which is also a cytosolic protein. To that end, we assessed TAGLN3 interaction with IκBα by following thermal denaturation of TAGLN3 in the presence of increasing concentrations of IκBα using differential scanning fluorimetry (nanoDSF) (Garnier et al., 2017). The progressive increase of free TAGLN3 denaturation temperature (T_m) from 56.8°C up to 61°C for TAGLN3 in the presence of 6-fold excess of IκBα unambiguously demonstrates the existence of such an interaction (Figure 6E). Fitting obtained data using a 1:1 model allowed us to estimate dissociation constant (K_D) of 10 μM. Thus, our results identified TAGLN3 as a functional downstream effector of APOE that modulates the inflammatory response as a regulator of NF-κB activity through its direct interaction with IκBα.

Downregulation of TAGLN3 mediates through histone deacetylation in APOE4 astrocytes

Next, we sought to identify upstream mechanisms by which APOE4 could regulate TAGLN3 expression. Previous reports have shown that SM22a/TAGLN transcription, in response to transforming growth factor β1 (TGF-β1), is dynamically regulated by changes in the histone acetylation state (Qiu et al., 2006). Histone acetylation levels at a gene regulatory sequence can be modified by HDACs that are therefore considered epigenomic regulators involved in downregulating gene expression (Chen et al., 2015). Noticeably, previous data have shown that APOE4 increases nuclear translocation of HDACs (Sen et al., 2015). Moreover, several HDACs were found to be increased in APOE-KO mice models (Manea et al., 2020). Our DNA microarray array also showed the upregulation of several HDACs in [*APOE4/E4*] human astrocytes such as HDACs 1/6/7/8/9/10, which was further confirmed by qPCR analyses for most of these HDACs (Figure S6A; Table S3). These observations prompted us to test whether TAGLN3 downregulation in APOE4 astrocytes could result from higher HDAC activity. [*APOE4/E4*] astrocytes were stimulated and treated with Vorinostat (SAHA), a broad inhibitor of HDAC activity. We found that TAGLN3 expression was significantly increased at both genic and proteic levels (Figures 7A, 7B, and S6B). As expected, parallel downregulation of the IL-6 and IL-8 inflammatory mediators was observed, ruling out a global non-specific effect of HDAC inhibition (Figures 7C and S6B). Thus, APOE could regulate TAGLN3 expression, at least partly, through HDAC-mediated epigenomic regulation.

TAGLN3 downregulation is a common trait in brains from patients with AD

Next, we measured TAGLN3 expression in hiPSC lines derived from patients with sAD and ND controls. We confirmed that TAGLN3 downregulation was strongly associated with the APOE4 polymorphism (Figures 7D and S7A–S7D). Furthermore, to unequivocally evaluate TAGLN3 as a potential target in AD, we assessed TAGLN3 expression in postmortem human brain tissues from patients with [*APOE3/E3*] and [*APOE4/E4*] sAD, as well as from the brains of [*APOE3/E3*] ND controls (Figure 7E; Table S4). Protein analyses revealed a significant TAGLN3 downregulation in the temporal cortex of patients with sAD who carried the [*APOE4/E4*] genotype (Figures 7F and 7G), ultimately confirming our initial discovery based on hiPSC astrocytes. Of further interest, we also found that TAGLN3 was significantly downregulated in the brain of aged patients with sAD carrying the [*APOE3/E3*] genotype (Figures 7F and 7G). The latter is parallel to our prior observation showing that, beside its chronic downregulation in APOE4 astrocytes, TAGLN3 downregulation can also occur in a pro-inflammatory context (Figure 6D), independently of APOE4. Taken together, our data could suggest that the pro-inflammatory environment in the brain of patients with late-stage AD might lead to TAGLN3 downregulation and further contribute to exacerbated inflammation. Non-exclusively, these data could also suggest that TAGLN3 downregulation is an early marker of glial dysfunctions, either as a consequence of a genetic trait or other factors such as aging, thus conferring a greater susceptibility to develop AD.

(B and C) Representative western blots (B) and quantitative analyses (C) for different members of the NF-κB pathway (as indicated) in [*APOE3/E3*] astrocytes (ND-1 [3/3], n = 1) and their respective isogenic [*APOE4/E4*]-KI (ND-1 KI [4/4], n = 3 independent lines) and *APOE*-KO (ND-1 KO, n = 3 independent lines) counterparts, with 3–6 independent batches of differentiation for each line. Cells were either treated with a pro-inflammatory cocktail (Stim+) or the control (Stim−). The "n" under each genotype indicates the total number of independent batches of differentiation analyzed and pooled for each condition.
(D) Representative images of [*APOE3/E3*] astrocytes and their respective [*APOE4/E4*]-KI astrocytes, in unstimulated (−) and stimulated (+) conditions, immunostained against p65 (green). Nuclei were counterstained with Hoechst (blue) to help the visualization of nuclear translocation.
Data are presented as mean ± SEM using one-way ANOVA followed by post hoc Dunnett's test (C). In (C), A.U. stands for arbitrary units. Scale bars: (D) 10 μm. For additional data and controls, see also Figure S4.

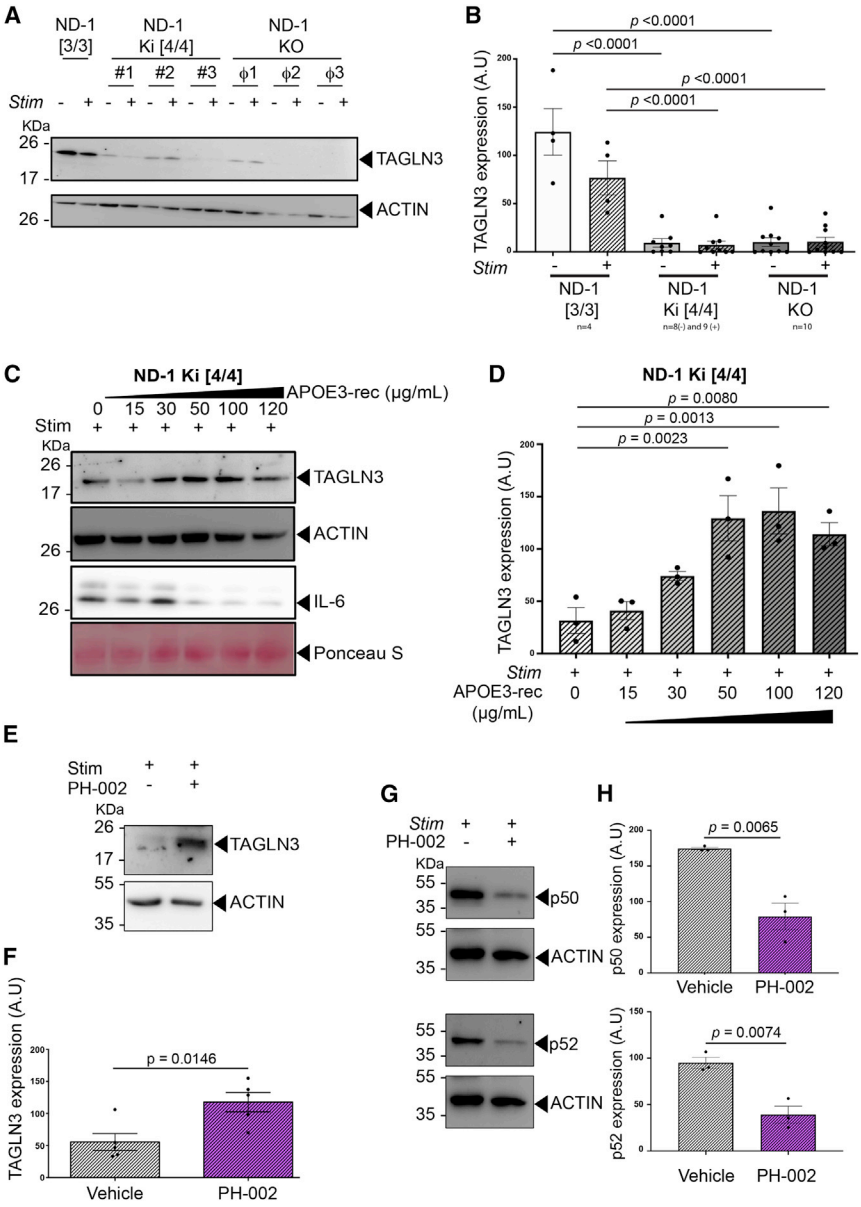

Figure 5. APOE4 downregulates TAGLN3 to promote pro-inflammation in human astrocytes via NF-κB activity

(A and B) Representative western blots (A) and quantification (B) of TAGLN3 from [*APOE3/E3*, n = 1], [*APOE4/E4*]-KI (n = 3 independent lines) and [*APOE*]-KO (n = 3 independent lines) astrocytes treated with a pro-inflammatory cocktail (Stim+) or a control (Stim−). The "n" under each genotype indicates the total number of independent batches of differentiation analyzed and pooled for each experimental condition.

(C and D) Representative western blots of TAGLN3 and IL-6 (C) and quantitative analyses (D) of TAGLN3 from [*APOE4/E4*]-Ki astrocytes (n = 3 independent lines) co-treated with a pro inflammatory Stim (Stim+) and the APOE3 recombinant protein (APOE3-rec) at different doses (n = 3/dose, with 1 batch of differentiation/line).

(E–G) [*APOE4/E4*]-Ki astrocytes (n = 3 independent lines) were co-treated with a pro-inflammatory cocktail (Stim) and the APOE4-structure corrector (PH-002, 100 µM), or its control vehicle, 24 h prior to being analyzed.

(E and F) Representative western blots (E) and quantitative analyses (F) for TAGLN3 (n = 5/condition, with 1–2 batches of differentiation/line).

(G and H) Representative Western blots (G) and quantitative analyses (H) for p50 and p52 (n = 3/condition, with 1batch of differentiation/line).

Data are presented as mean ± SEM using one-way ANOVA followed by post hoc Dunnett's test (B and D) or using unpaired two-tailed Student's t test (F and H). In (B), (D), (F), and (H), A.U. stands for arbitrary units (see STAR Methods).

For additional data and controls, see also Figure S5.

DISCUSSION

APOE has been previously associated with both pro- and anti-inflammatory responses in various pathological contexts, highlighting its intricate roles on inflammation. Several pieces of evidence have suggested that APOE4 confers a higher risk for developing CNS diseases through dysfunctions affecting the neuroinflammatory mechanisms in glial cells (Yin et al., 2019; Serrano-Pozo et al., 2021; Tzioras et al., 2019; Guo et al., 2004), but the exact mechanisms remained unclear. Our results demonstrate the key role of APOE in modulating the inflammatory response in human astrocytes and highlight the APOE4 variant as a key driver of (1) low-grade chronic inflammation and (2) exacerbated responses to cytokine stimuli that recapitulate the AD environment. Highlighting a regulatory mechanism of APOE on NF-κB-mediated neuroinflammation, our data further support the importance of APOE in the control of inflammation. In line with recent observations that demonstrate the key role of APOE in the control of the complement cascade (Yin et al., 2019), our results show that APOE can achieve this critical function through distinct and non-exclusive mechanisms. Based on the described repression of SM22/TAGLN expression in APOE-deficient mice and the concomitant loss of its inhibitory effect on NF-κB activity (Dai et al., 2017; Shen et al., 2010), we identified a brain-specific member of the transgelin family, TAGLN3, as a target of APOE. Indeed, we show that the APOE4-dependent repression of TAGLN3 is a mechanism responsible for the increased basal and cytokine-induced expression of inflammation-related genes in human astrocytes, which involves the loss of regulation of the NF-κB pathway. Accordingly, this mechanism could be of major importance in modulating the risk of AD since NF-κB has emerged as a regulator of aging and its over-activation was described in a number of age-associated diseases (Tilstra et al., 2011). Importantly, we also showed that TAGLN3 downregulation is not exclusively driven by APOE4, as this was also found in the brain of aged patients with sAD, independently of the APOE4 genotype. Thus,

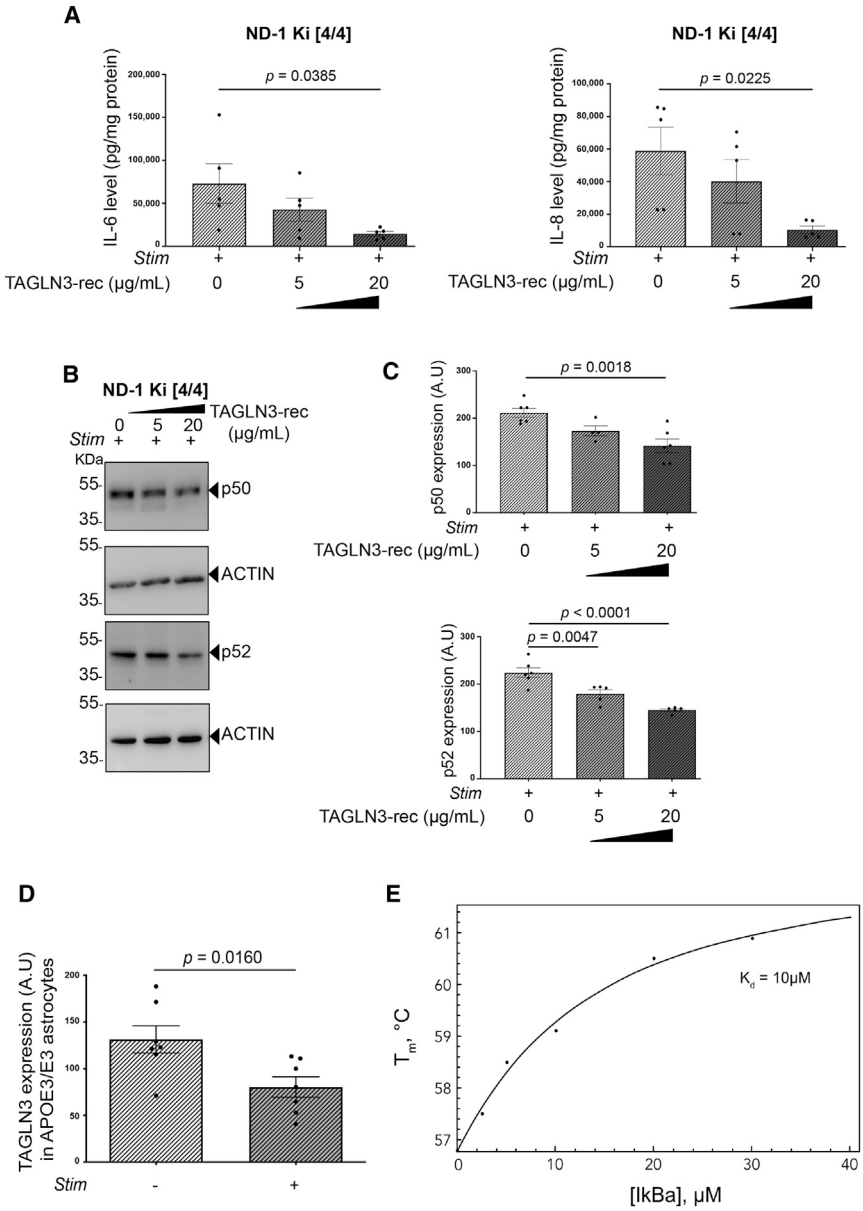

Figure 6. TAGLN3 exerts a control of inflammation in human astrocytes by interacting with IκBα to negatively regulate NF-κB activity

(A) Quantification by ELISA of IL-6 and IL-8 from stimulated [*APOE4/E4*]-Ki astrocytes (n = 3 independent lines) co-treated with two different doses of TAGLN3 (5 and 20 µg/mL), as recombinant protein (TAGLN3-rec) (n = 5/dose, with 1–2 independent batches of differentiation/line).

(B and C) Representative western blots (B) and quantitative analyses (C) of P50 and P52 from [*APOE4/E4*]-Ki astrocytes (n = 3 lines) co-treated with a pro inflammatory Stim (Stim+) and the TAGLN3 recombinant protein (TAGLN3-rec) at different doses (n = 4–6/dose, with 1–2 independent batches of differentiation/line).

(D) Quantification of TAGLN3 from stimulated and non-stimulated [*APOE3/E3*] astrocytes by western blot analysis (n = 7 independent batches of differentiation).

(E) Denaturation temperature (T_m) of TAGLN3 in the presence of increasing concentrations of IκBα (0–40 µM) was measured using nanoDSF (black dots). Data were fitted (solid line) using one-t-one binding model. Data are presented as mean ± SEM using one-way ANOVA followed by post hoc Dunnett's test (A and C) or using unpaired two-tailed Student's t test (D). In (C) and (D), A.U. stands for arbitrary units (see STAR Methods).

TAGLN3 downregulation may also be driven by other mechanisms brought on by age advancement. For example, we showed that TAGLN3 expression is reduced in cytokine-stimulated APOE3 astrocytes, thus suggesting that TAGLN3 repression may also be representative of a chronic inflammatory state. Taken together, these data suggest that TAGLN3 downregulation in human astrocytes might be an important mechanism underlying age-associated changes in brain. Thus, TAGLN3 downregulation in astrocytes might be a bridging molecular mechanism underlying APOE4- or aging-associated alterations affecting neuroinflammatory functions in astrocytes. This might participate to predispose the brain to a higher risk of developing neuronal-associated pathological phenotypes through chronic and/or excessive production of pro-inflammatory mediators in response to inflammatory events throughout life. In the future, it would be interesting to evaluate whether TAGLN3 downregulation in *APOE*ε4 carriers accelerates the pace of biological neuroimmune aging, which may have major implications in AD and other age-related disorders, as recently described (Elliott et al., 2021; Cullen et al., 2021). Furthermore, APOE4 could also negatively impact on the worsening of the disease by other pathological mechanisms such as amyloidogenesis and tauopathy in AD, as already described (Liu et al., 2017; Shi et al., 2017). Previous studies have demonstrated that the APOE4 structure is involved in changes related to these two pathological hallmarks in AD, which can be ameliorated with the use of an APOE4-structure corrector, PH-002 (Chen et al., 2012). Thus, the Huang laboratory showed that the use of PH-002 lowers Aβ production and the levels of phosphorylated tau in APOE4 hiPSC neurons, as well as reduces GABAergic neuron degeneration (Wang et al., 2018). Supporting further the critical role of the APOE4 structure in the pathology, our data showed that PH-002 can also rescue the pro-inflammatory phenotype observed in astrocytes. This suggests that the conformational structure of APOE4 also determines functional changes driving inflammation in astrocytes, but the exact mechanism(s) remained yet undetermined. These results pave the way toward correcting the pathogenic confirmation of APOE4 as an approach to modulate multiple and key pathological processes,

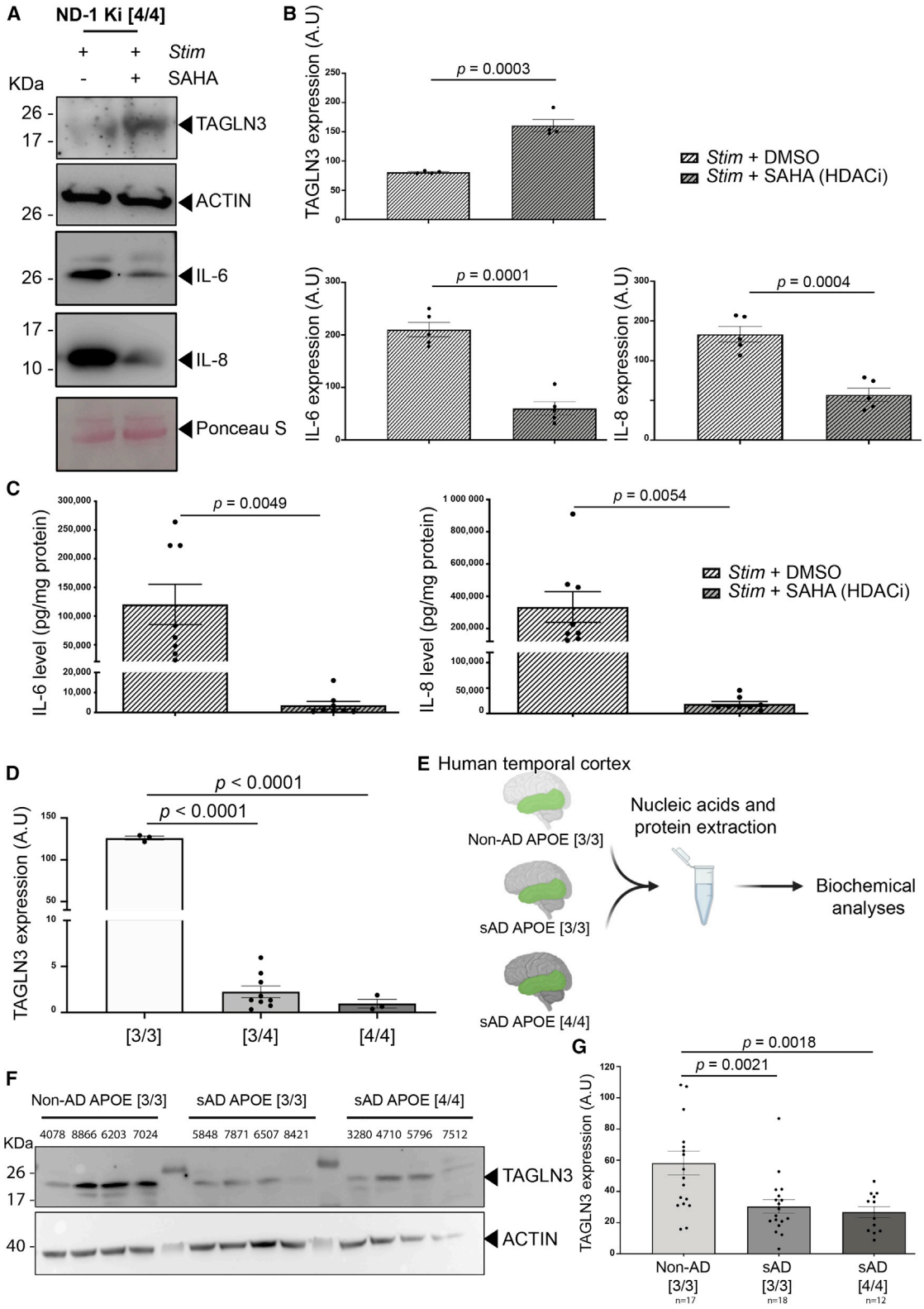

Figure 7. TAGLN3 downregulation, a feature found in human AD brains, involves HDACs activity in APOE4 astrocytes

(A and B) [*APOE4/E4*]-Ki astrocytes (n = 3 independent lines) were treated with the broad-spectrum HDAC inhibitor SAHA or with DMSO as control. Cells were stimulated with a pro-inflammatory cocktail (Stim) and evaluated for TAGLN3, IL-6, and IL-8 expression. Representative western blots (A) and quantitative

(legend continued on next page)

in multiple cell types, for APOE4-related AD pathology. Altogether, our study emphasizes the necessity for a critical reconsideration of the sequence of the events underlying pathogenesis, as early glial cell dysfunctions could precede the toxic accumulation of Aβ, at least in some cases, and so the neuronal pathology.

TAGLN3 is a member of the transgelin family preferentially expressed in the CNS, but very little is known about its functions. This protein shares homology with another transgelin member, namely SM22a/TAGLN, which is abundant in VSMCs of vertebrates (Lees-Miller et al., 1987). Although the role of TAGLN3 is much less documented than TAGLN2 and SM22a/TAGLN, they all belong to the calponin family and could be involved in cytoskeleton organization as actin-binding proteins (Thompson et al., 2012; Fu et al., 2000). Current knowledge on TAGLN3, also known as neuronal protein 22 (NP22), are strictly limited to a possible role in neuronal architecture through its domains, consistent with those of cytoskeletal-interacting proteins (Depaz and Wilce, 2006; Depaz et al., 2005). A role for TAGLN3 on the astrocyte architecture cannot be excluded and will require further investigations. This is of utmost importance considering the role of the cytoskeletal machinery behind the dynamic shape changes of astrocyte morphology that drive tissue remodeling during pathogenic processes (Schiweck et al., 2018). However, this is unlikely, as we found TAGLN3 in the cytosol and the nucleus of astrocytes but not in the cytoskeleton, suggesting that TAGLN3 may have different functions in neurons and astrocytes. Interestingly, we showed that exogenous application of TAGLN3 could rescue the disease phenotype observed in APOE4 astrocytes. Therefore, and considering the cross-talk between astrocytes and neurons, it would also be interesting to evaluate whether neuronal TAGLN3 could be released and impact astrocytes. Up to now, no previous functions had ever been ascribed to TAGLN3 in astrocytes. In this study, we identified TAGLN3 as a regulator of inflammation in astrocytes. The inhibitory effect of TAGLN3 on NF-κB activity can be deduced from reports highlighting the role of SM22 in its inhibition at the periphery (Dai et al., 2017; Shen et al., 2010). The protein-ligand interaction we showed between TAGLN3 and IκBα suggests that TAGLN3 may play an important role to negatively regulate NF-κB activity in human astrocytes. We also identified TAGLN3 as a main protein downstream of APOE, involving a control through HDAC activity, enabling the modulation of the inflammatory responses from human astrocytes. Herein, we demonstrate that APOE4-dependent repression of TAGLN3 was triggered by HDAC activities. Interestingly, HDAC expression was shown to increase with age in the brain (Gilbert et al., 2019). This could place HDAC-mediated epigenomic changes as a unifying mechanism between APOE4 and aging that might contribute to drive astroglial immune dysfunctions, but at a different pace, and predispose the brain for age-related disorders such as AD through TAGLN3 repression.

Finally, our study revealed that pharmacological targeting of TAGLN3 is a valid approach to modulate neuroinflammation in astrocytes and probably a better approach as opposed to upstream modulation of APOE that has a broad spectrum of actions. Of utmost importance, combined with our *in vitro* observations, our data in human brain samples support TAGLN3 downregulation as a possible biomarker in AD. This is especially true if we consider that TAGLN3 has already been detected in cerebrospinal fluid (CSF) (Guldbrandsen et al., 2014). Indeed, monitoring TAGLN3 downregulation in individuals could help identify early asymptomatic stages and/or increased risk to develop the disease, as observed in *APOE4* carriers. Of further interest would be to evaluate whether TAGLN3 levels correlate with different clinical stages. Interestingly, a recent transcriptomic study with spatial resolution has identified TAGLN3 as a member of a new hub of genes downregulated in the middle temporal gyrus in aged patients with AD diagnosed at early stage (Braak III–IV) and linked to glial cells (Chen et al., 2021). These recent data further support the relevance of TAGLN3 downregulation as an early bridging mechanism between aging, inflammation, and AD pathology. This places TAGLN3 downregulation as a potential biomarker to predict a risk for AD and will require further investigations. In the future, developing TAGLN3-targeting strategies could ultimately facilitate the development of prophylactic therapies or early intervention in a stratified population at risk for numerous age-related brain diseases. Such an approach could lead to a first-in-class, far-reaching therapeutic eventually benefiting *APOE*ε4 carriers at least, which represent nearly 15% of the worldwide population.

Limitations of the study

While we demonstrated that APOE4 drives a pro-inflammatory phenotype in human astrocytes through TAGLN3 downregulation, this study still has several limitations. First, our observations

analyses (B) for TAGLN3 (n = 4/condition, with 1–2 independent batches of differentiation/line), IL-6, and IL-8 expression (n = 5/condition, with 1–2 independent batches of differentiation/line).

(C) IL-6 and IL-8 levels were assessed by ELISA from the supernatants of the different cultures/conditions (n = 8/condition, with 2–3 independent batches of differentiation/line).

(D) Graph chart showing quantitative measurements from western blot analyses for TAGLN3 from multiple patient-specific astrocytes with different APOE genotypes. Astrocytes from one [*APOE3/E3*], three [*APOE3/E4*], and one [*APOE4/E4*] patient-specific lines were analyzed, with 3 independent batches of differentiation for each line (n = 3, 9, and 3, respectively).

(E) Illustration depicting the experimental procedure used to analyze the TAGLN3 expression from postmortem human brain samples as follows: not diagnosed for AD (non-AD, [*APOE3/E3*] n = 6) or diagnosed for AD (sAD, [*APOE3/E3*] n = 6 or [*APOE4/E4*] n = 4).

(F and G) Representative western blot (F) and quantitative analysis (G) for TAGLN3 expression in the temporal cortex from the three different groups of patients as aforementioned. For each APOE genotype, 2–3 independent technical replicates from a same patient have been analyzed. The "n" under each genotype indicates the total number of independent replicates analyzed and pooled. Of note, the indicated numbers referred to the unique sample ID from each patient.

Data are presented as mean ± SEM using unpaired two-tailed Student's t test (B and C) or one-way ANOVA followed by post hoc Dunnett's test (D and G). In (B), (D), and (G), A.U. stands for arbitrary units (see STAR Methiods).

For additional data and controls, see also Figures S6 and S7.

are mainly based on hiPSC-derived astrocytes, which may require further validation from primary human astrocytes. Moreover, the hiPSC-based model we used does not reproduce the entire brain complexity where astrocytes interact with numerous other cell types, including neurons, which could participate to modulate this phenotype. Second, even though we identified the NF-κB activity as one of the mechanisms underlying the pro-inflammatory phenotype in APOE4 astrocytes, we cannot rule out that other mechanisms/pathways are also involved. Deeper analyses of other signaling pathways found altered in APOE4 astrocytes will help identify other pro-inflammatory mechanisms. Third, the HDAC-mediated control of APOE on the TAGLN3 expression was indirectly demonstrated. More mechanistic studies would be required to ultimately demonstrate how the APOE4 isoform affects TAGLN3 expression through epigenomic remodeling. Lastly, postmortem human brain analyses were performed on temporal cortex. A more thorough analyses on other brain regions would be required, and proteomic-based approaches would be additionally recommended to validate further our observations and investigate TAGLN3 as a biomarker in AD.

STAR★METHODS

Detailed methods are provided in the online version of this paper and include the following:

- KEY RESOURCES TABLE
- RESOURCE AVAILABILITY
  - Lead contact
  - Material availability
  - Data and code availability
- EXPERIMENTAL MODEL AND SUBJECT DETAILS
  - Human iPS cells (hiPSC)
  - Human *post-mortem* brain tissues
- METHOD DETAILS
  - Culture of human iPSC (hiPSC) lines
  - Differentiation of neural progenitors cells (NPCs) from hiPSCs
  - Differentiation of astrocytes-like cells from NPCs
  - CRISPR/Cas9 gene correction
  - Karyotyping
  - Astrocytes treatment
  - DNA microarray
  - Total RNA isolation and quantitative real-time PCR analysis for mRNA expression
  - Sub-cellular fractionation
  - Immunoblotting and protein quantification
  - ELISA procedure
  - Differential scanning fluorimetry (DSF)
  - Human brain tissues analysis
  - Immunofluorescence labelling experiments
- QUANTIFICATION AND STATISTICAL ANALYSIS

SUPPLEMENTAL INFORMATION

Supplemental information can be found online at https://doi.org/10.1016/j.celrep.2022.111200.

ACKNOWLEDGMENTS

This work was supported by the CNRS and Aix Marseille Université. The work was also supported by the DHUNE Center of Excellence and a CoEN grant (to S.R. and E.N.), by the "FONDATION ALZHEIMER" (to S.R. and E.N.), by "Fondation Vaincre Alzheimer" (FR-19052 to E.N.), by "La Fondation NRJ-Institut de France" to E.N., by l'Agence Nationale de la Recherche (ANR) (ANR-21-CE17-0047-01 to E.N.), and by a CoEN grant to S.R. and E.N. L.G.-G. was supported by an ANR grant (MAD5) to S.R. and also by grants from the Fondation pour la Recherche Médicale FRM FDT201904008423 and by a Fondation Vaincre Alzheimer international travel grant. This work has received support from the French government under the Programme Investissements d'Avenir, Initiative d'Excellence d'Aix-Marseille Université via A*Midex (AMX-19-IET-004) and ANR (ANR-17-EURE-0029) funding.

All human brain samples used in the study were kindly provided by the Brainbank Neuro-CEB Neuropathology Network, which includes Dr. Franck Letournel (CHU Angers), Dr. Marie-Laure Martin-Négrier (CHU Bordeaux), Prof. Françoise Chapon (CHU Caen), Prof. Catherine Godfraind (CHU Clermont-Ferrand), Prof. Claude-Alain Maurage (CHU Lille), Dr. Vincent Deramecourt (CHU Lille), Dr. David Meyronnet (CHU Lyon), Dr. Nathalie Streichenberger (CHU Lyon), Dr. André Maues de Paula (CHU Marseille), Prof. Valérie Rigau (CHU Montpellier), Dr. Fanny Vandenbos-Burel (Nice), Prof. Charles Duyckaerts (CHU PS Paris), Prof. Danielle Seilhean (CHU PS, Paris), Dr. Susana Boluda (CHU PS, Paris), Dr. Isabelle Plu (CHU PS, Paris), Dr. Serge Milin (CHU Poitiers), Dr. Dan Christian Chiforeanu (CHU Rennes), Prof. Annie Laquerrière (CHU Rouen), and Dr. Béatrice Lannes (CHU Strasbourg). We thank Dr. Aurélie Tchoghandjian Auphan and Thomas Perez for providing us with antibodies against members of the NF-κB pathway and the SAHA compound, respectively. We acknowledge the support and expertise of the NeuroTimone Platforms (PFNT) of the INP, in particular the Neuro Cellular Imaging Service (NCIS), the Interactome Timone Platforms (PINT), and the Stem Cell Center NeuroTimone (SCeNT), labeled by Aix Marseille University (AMIDEX), the CNRS, and Inserm and financed in part by the FEDER and a state-reginal contract. For karyotyping analysis, this work has obtained technical support from the Chromostem platform (CHRU of Montpellier, France), providing all necessary equipment and the technical expertise of Pr. Franck Pellestor (f-pellestor@chu-montpellier.fr), who is the scientific manager of the platform. Schematic illustrations used in this study are unique and were created from the BioRender.com website.

AUTHOR CONTRIBUTIONS

L.A. and E.N. designed and conceived the whole study. P.B., J.C.I.B., I.S.-M., K.B., and S.R. advised on some experiments. L.A., L.G., and D.S. performed all experiments and collected and analyzed the data. L.A., K.B., S.R., and E.N. interpreted the data. P.B. performed DNA microarray and pathway analyses and interpreted the microarray data. A.J. performed cell culture experiments, western blot analyses, and image acquisitions. L.A., L.G., L.G.-G., and N.J. contributed to CRISPR-Cas9 design and plasmid constructions. F.D. and P.O.T. performed nanoDSF experiments. J.C.I.B. advised and provided training for CRISPR-Cas9 experiments. E.N. wrote the original manuscript. L.A., P.B., L.G., I.S.-M., J.C.I.B., S.R., and E.N. assisted with review and editing of the manuscript. E.N. supervised all studies and manuscript preparation. All authors reviewed the manuscript and approved the final version.

DECLARATION OF INTERESTS

The authors declare no competing interests.

Received: December 17, 2021
Revised: May 23, 2022
Accepted: July 21, 2022
Published: August 16, 2022

REFERENCES

Arranz, A.M., and De Strooper, B. (2019). The role of astroglia in Alzheimer's disease: pathophysiology and clinical implications. Lancet Neurol. *18*, 406–414. https://doi.org/10.1016/S1474-4422(18)30490-3.

Blasko, I., Marx, F., Steiner, E., Hartmann, T., and Grubeck-Loebenstein, B. (1999). TNFα plus IFNγ induce the production of Alzheimer β-amyloid peptides and decrease the secretion of APPs. FASEB. J. *13*, 63–68. https://doi.org/10.1096/fasebj.13.1.63.

Ceyzériat, K., Ben Haim, L., Denizot, A., Pommier, D., Matos, M., Guillemaud, O., Palomares, M.-A., Abjean, L., Petit, F., Gipchtein, P., et al. (2018). Modulation of astrocyte reactivity improves functional deficits in mouse models of Alzheimer's disease. Acta Neuropathol. Commun. *6*, 104. https://doi.org/10.1186/s40478-018-0606-1.

Chambers, S.M., Fasano, C.A., Papapetrou, E.P., Tomishima, M., Sadelain, M., and Studer, L. (2009). Highly efficient neural conversion of human ES and iPS cells by dual inhibition of SMAD signaling. Nat. Biotechnol. *27*, 275–280. https://doi.org/10.1038/nbt.1529.

Chen, H.-K., Liu, Z., Meyer-Franke, A., Brodbeck, J., Miranda, R.D., McGuire, J.G., Pleiss, M.A., Ji, Z.-S., Balestra, M.E., Walker, D.W., et al. (2012). Small molecule structure correctors abolish detrimental effects of apolipoprotein E4 in cultured neurons. J. Biol. Chem. *287*, 5253–5266. https://doi.org/10.1074/jbc.M111.276162.

Chen, H.P., Zhao, Y.T., and Zhao, T.C. (2015). Histone deacetylases and mechanisms of regulation of gene expression. Crit. Rev. Oncog. *20*, 35–47. https://doi.org/10.1615/critrevoncog.2015012997.

Chen, S., Chang, Y., Li, L., Acosta, D., Morrison, C., Wang, C., Julian, D., Hester, M.E., Serrano, G.E., Beach, T.G., et al. (2021). Spatially resolved transcriptomics reveals unique gene signatures associated with human temporal cortical architecture and Alzheimer's pathology. Preprint at bioRxiv. https://doi.org/10.1101/2021.07.07.451554.

Corder, E.H., Saunders, A.M., Strittmatter, W.J., Schmechel, D.E., Gaskell, P.C., Small, G.W., Roses, A.D., Haines, J.L., and Pericak-Vance, M.A. (1993). Gene dose of apolipoprotein E type 4 allele and the risk of Alzheimer's disease in late onset families. Science *261*, 921–923. https://doi.org/10.1126/science.8346443.

Cullen, N.C., Mälarstig, A.N., Stomrud, E., Hansson, O., and Mattsson-Carlgren, N. (2021). Accelerated inflammatory aging in Alzheimer's disease and its relation to amyloid, tau, and cognition. Sci. Rep. *11*, 1965. https://doi.org/10.1038/s41598-021-81705-7.

Dai, X., Thiagarajan, D., Fang, J., Shen, J., Annam, N.P., Yang, Z., Jiang, H., Ju, D., Xie, Y., Zhang, K., et al. (2017). SM22α suppresses cytokine-induced inflammation and the transcription of NF-κB inducing kinase (Nik) by modulating SRF transcriptional activity in vascular smooth muscle cells. PLoS One *12*, e0190191. https://doi.org/10.1371/journal.pone.0190191.

Depaz, I.M., and Wilce, P.A. (2006). The novel cytoskeleton-associated protein Neuronal protein 22: elevated expression in the developing rat brain. Brain Res. *1081*, 59–64. https://doi.org/10.1016/j.brainres.2006.01.126.

Depaz, I.M., de las Heras, R., Kroon, P.A., and Wilce, P.A. (2005). Changes in neuronal protein 22 expression and cytoskeletal association in the alcohol-dependent and withdrawn rat brain. J. Neurosci. Res. *81*, 253–260. https://doi.org/10.1002/jnr.20563.

Dominy, S.S., Lynch, C., Ermini, F., Benedyk, M., Marczyk, A., Konradi, A., Nguyen, M., Haditsch, U., Raha, D., Griffin, C., et al. (2019). *Porphyromonas gingivalis* in Alzheimer's disease brains: evidence for disease causation and treatment with small-molecule inhibitors. Sci. Adv. *5*, eaau3333. https://doi.org/10.1126/sciadv.aau3333.

Elliott, M.L., Caspi, A., Houts, R.M., Ambler, A., Broadbent, J.M., Hancox, R.J., Harrington, H., Hogan, S., Keenan, R., Knodt, A., et al. (2021). Disparities in the pace of biological aging among midlife adults of the same chronological age have implications for future frailty risk and policy. Nat. Aging *1*, 295–308. https://doi.org/10.1038/s43587-021-00044-4.

Fu, Y., Liu, H.W., Forsythe, S.M., Kogut, P., McConville, J.F., Halayko, A.J., Camoretti-Mercado, B., and Solway, J. (2000). Mutagenesis analysis of human SM22: characterization of actin binding. J. Appl. Physiol. *89*, 1985–1990. https://doi.org/10.1152/jappl.2000.89.5.1985.

Furman, J.L., Sama, D.M., Gant, J.C., Beckett, T.L., Murphy, M.P., Bachstetter, A.D., Van Eldik, L.J., and Norris, C.M. (2012). Targeting astrocytes ameliorates neurologic changes in a mouse model of Alzheimer's disease. J. Neurosci. *32*, 16129–16140. https://doi.org/10.1523/JNEUROSCI.2323-12.2012.

Garnier, C., Devred, F., Byrne, D., Puppo, R., Roman, A.Y., Malesinski, S., Golovin, A.V., Lebrun, R., Ninkina, N.N., and Tsvetkov, P.O. (2017). Zinc binding to RNA recognition motif of TDP-43 induces the formation of amyloid-like aggregates. Sci. Rep. *7*, 6812. https://doi.org/10.1038/s41598-017-07215-7.

Gilbert, T.M., Zürcher, N.R., Catanese, M.C., Tseng, C.-E.J., Di Biase, M.A., Lyall, A.E., Hightower, B.G., Parmar, A.J., Bhanot, A., Wu, C.J., et al. (2019). Neuroepigenetic signatures of age and sex in the living human brain. Nat. Commun. *10*, 2945. https://doi.org/10.1038/s41467-019-11031-0.

Giovannoni, F., and Quintana, F.J. (2020). The role of astrocytes in CNS inflammation. Trends Immunol. *41*, 805–819. https://doi.org/10.1016/j.it.2020.07.007.

Guldbrandsen, A., Vethe, H., Farag, Y., Oveland, E., Garberg, H., Berle, M., Myhr, K.-M., Opsahl, J.A., Barsnes, H., and Berven, F.S. (2014). In-depth characterization of the cerebrospinal fluid (CSF) Proteome displayed through the CSF Proteome resource (CSF-PR). Mol. Cell. Proteomics *13*, 3152–3163. https://doi.org/10.1074/mcp.M114.038554.

Guo, L., LaDu, M.J., and Van Eldik, L.J. (2004). A dual role for apolipoprotein E in neuroinflammation: anti- and pro-inflammatory activity. J. Mol. Neurosci. *23*, 205–212. https://doi.org/10.1385/JMN:23:3:205.

Hu, W.T., Howell, J.C., Ozturk, T., Gangishetti, U., Kollhoff, A.L., Hatcher-Martin, J.M., Anderson, A.M., and Tyor, W.R. (2019). CSF cytokines in aging, multiple sclerosis, and dementia. Front. Immunol. *10*, 480. https://doi.org/10.3389/fimmu.2019.00480.

Huang, Y., and Mahley, R.W. (2014). Apolipoprotein E: structure and function in lipid metabolism, neurobiology, and Alzheimer's diseases. Neurobiol. Dis. *72 Pt A*, 3–12. https://doi.org/10.1016/j.nbd.2014.08.025.

Huang, Y.-W.A., Zhou, B., Wernig, M., and Südhof, T.C. (2017). ApoE2, ApoE3, and ApoE4 differentially stimulate APP transcription and Aβ secretion. Cell *168*, 427–441.e21. https://doi.org/10.1016/j.cell.2016.12.044.

Hüll, M., Strauss, S., Berger, M., Volk, B., and Bauer, J. (1996). The participation of interleukin-6, a stress-inducible cytokine, in the pathogenesis of Alzheimer's disease. Behav. Brain Res. *78*, 37–41. https://doi.org/10.1016/0166-4328(95)00213-8.

Ito, M., Depaz, I., Wilce, P., Suzuki, T., Niwa, S.i., and Matsumoto, I. (2005). Expression of human neuronal protein 22, a novel cytoskeleton-associated protein, was decreased in the anterior cingulate cortex of schizophrenia. Neurosci. Lett. *378*, 125–130. https://doi.org/10.1016/j.neulet.2004.12.079.

Jeong, J.-Y., Yim, H.-S., Ryu, J.-Y., Lee, H.S., Lee, J.-H., Seen, D.-S., and Kang, S.G. (2012). One-step sequence- and ligation-independent cloning as a rapid and versatile cloning method for functional genomics studies. Appl. Environ. Microbiol. *78*, 5440–5443. https://doi.org/10.1128/AEM.00844-12.

Kinney, J.W., Bemiller, S.M., Murtishaw, A.S., Leisgang, A.M., Salazar, A.M., and Lamb, B.T. (2018). Inflammation as a central mechanism in Alzheimer's disease. Alzheimers Dement. *4*, 575–590. https://doi.org/10.1016/j.trci.2018.06.014.

Kunkle, B.W., Grenier-Boley, B., Sims, R., Bis, J.C., Damotte, V., Naj, A.C., Boland, A., Vronskaya, M., van der Lee, S.J., Amlie-Wolf, A., et al. (2019). Genetic meta-analysis of diagnosed Alzheimer's disease identifies new risk loci and implicates Aβ, tau, immunity and lipid processing. Nat. Genet. *51*, 414–430. https://doi.org/10.1038/s41588-019-0358-2.

Lees-Miller, J.P., Heeley, D.H., and Smillie, L.B. (1987). An abundant and novel protein of 22 kDa (SM22) is widely distributed in smooth muscles. Purification from bovine aorta. Biochem. J. *244*, 705–709. https://doi.org/10.1042/bj2440705.

Lin, Y.-T., Seo, J., Gao, F., Feldman, H.M., Wen, H.-L., Penney, J., Cam, H.P., Gjoneska, E., Raja, W.K., Cheng, J., et al. (2018). APOE4 causes widespread

molecular and cellular alterations associated with Alzheimer's disease phenotypes in human iPSC-derived brain cell types. Neuron *98*, 1141–1154.e7. https://doi.org/10.1016/j.neuron.2018.05.008.

Liu, C.-C., Zhao, N., Fu, Y., Wang, N., Linares, C., Tsai, C.-W., and Bu, G. (2017). ApoE4 accelerates early seeding of amyloid pathology. Neuron *96*, 1024–1032.e3. https://doi.org/10.1016/j.neuron.2017.11.013.

Manea, S.-A., Vlad, M.-L., Fenyo, I.M., Lazar, A.-G., Raicu, M., Muresian, H., Simionescu, M., and Manea, A. (2020). Pharmacological inhibition of histone deacetylase reduces NADPH oxidase expression, oxidative stress and the progression of atherosclerotic lesions in hypercholesterolemic apolipoprotein E-deficient mice; potential implications for human atherosclerosis. Redox Biol. *28*, 101338. https://doi.org/10.1016/j.redox.2019.101338.

Martorana, A., Bulati, M., Buffa, S., Pellicanò, M., Caruso, C., Candore, G., and Colonna-Romano, G. (2012). Immunosenescence, inflammation and Alzheimer's disease. Longev. Healthspan *1*, 8. https://doi.org/10.1186/2046-2395-1-8.

Montagne, A., Nikolakopoulou, A.M., Huuskonen, M.T., Sagare, A.P., Lawson, E.J., Lazic, D., Rege, S.V., Grond, A., Zuniga, E., Barnes, S.R., et al. (2021). APOE4 accelerates advanced-stage vascular and neurodegenerative disorder in old Alzheimer's mice via cyclophilin A independently of amyloid-β. Nat. Aging *1*, 506–520. https://doi.org/10.1038/s43587-021-00073-z.

Neff, M.M., Neff, J.D., Chory, J., and Pepper, A.E. (1998). dCAPS, a simple technique for the genetic analysis of single nucleotide polymorphisms: experimental applications in *Arabidopsis thaliana* genetics. Plant J. *14*, 387–392. https://doi.org/10.1046/j.1365-313X.1998.00124.x.

Patatian, A., and Benech, P. (2020). Identifying potential Clues on Covid-19 through Coronavirus-related literature using A data-driven approach with the help of A text mining-based software, PredictSearch. IJSRP *10*, 515–524. https://doi.org/10.29322/IJSRP.10.09.2020.p10560.

Pitas, R.E., Boyles, J.K., Lee, S.H., Foss, D., and Mahley, R.W. (1987). Astrocytes synthesize apolipoprotein E and metabolize apolipoprotein E-containing lipoproteins. Biochim. Biophys. Acta *917*, 148–161. https://doi.org/10.1016/0005-2760(87)90295-5.

Qiu, P., Ritchie, R.P., Gong, X.Q., Hamamori, Y., and Li, L. (2006). Dynamic changes in chromatin acetylation and the expression of histone acetyltransferases and histone deacetylases regulate the SM22alpha transcription in response to Smad3-mediated TGFbeta1 signaling. Biochem. Biophys. Res. Commun. *348*, 351–358. https://doi.org/10.1016/j.bbrc.2006.07.009.

Ran, F.A., Hsu, P.D., Wright, J., Agarwala, V., Scott, D.A., and Zhang, F. (2013). Genome engineering using the CRISPR-Cas9 system. Nat. Protoc. *8*, 2281–2308. https://doi.org/10.1038/nprot.2013.143.

Rodriguez, G.A., Tai, L.M., LaDu, M.J., and Rebeck, G.W. (2014). Human APOE4 increases microglia reactivity at Aβ plaques in a mouse model of Aβ deposition. J. Neuroinflammation *11*, 111. https://doi.org/10.1186/1742-2094-11-111.

Schiweck, J., Eickholt, B.J., and Murk, K. (2018). Important shapeshifter: mechanisms allowing astrocytes to respond to the changing nervous system during development, injury and disease. Front. Cell. Neurosci. *12*, 261. https://doi.org/10.3389/fncel.2018.00261.

Schöll, M., Carter, S.F., Westman, E., Rodriguez-Vieitez, E., Almkvist, O., Thordardottir, S., Wall, A., Graff, C., Långström, B., and Nordberg, A. (2015). Early astrocytosis in autosomal dominant Alzheimer's disease measured in vivo by multi-tracer positron emission tomography. Sci. Rep. *5*, 16404. https://doi.org/10.1038/srep16404.

Selkoe, D.J., and Hardy, J. (2016). The amyloid hypothesis of Alzheimer's disease at 25 years. EMBO Mol. Med. *8*, 595–608. https://doi.org/10.15252/emmm.201606210.

Sen, A., Nelson, T.J., and Alkon, D.L. (2015). ApoE4 and Aβ oligomers reduce BDNF expression via HDAC nuclear translocation. J. Neurosci. *35*, 7538–7551. https://doi.org/10.1523/JNEUROSCI.0260-15.2015.

Serrano-Pozo, A., Li, Z., Noori, A., Nguyen, H.N., Mezlini, A., Li, L., Hudry, E., Jackson, R.J., Hyman, B.T., and Das, S. (2021). Effect of APOE alleles on the glial transcriptome in normal aging and Alzheimer's disease. Nat. Aging *1*, 919–931. https://doi.org/10.1038/s43587-021-00123-6.

Shen, J., Yang, M., Ju, D., Jiang, H., Zheng, J.-P., Xu, Z., and Li, L. (2010). Disruption of SM22 promotes inflammation after artery injury via nuclear factor κB activation. Circ. Res. *106*, 1351–1362. https://doi.org/10.1161/CIRCRESAHA.109.213900.

Shi, Y., and Holtzman, D.M. (2018). Interplay between innate immunity and Alzheimer disease: APOE and TREM2 in the spotlight. Nat. Rev. Immunol. *18*, 759–772. https://doi.org/10.1038/s41577-018-0051-1.

Shi, Y., Yamada, K., Liddelow, S.A., Smith, S.T., Zhao, L., Luo, W., Tsai, R.M., Spina, S., Grinberg, L.T., Rojas, J.C., et al. (2017). ApoE4 markedly exacerbates tau-mediated neurodegeneration in a mouse model of tauopathy. Nature *549*, 523–527. https://doi.org/10.1038/nature24016.

Sofroniew, M.V., and Vinters, H.V. (2010). Astrocytes: biology and pathology. Acta Neuropathol. *119*, 7–35. https://doi.org/10.1007/s00401-009-0619-8.

Sutinen, E.M., Pirttilä, T., Anderson, G., Salminen, A., and Ojala, J.O. (2012). Pro-inflammatory interleukin-18 increases Alzheimer's disease-associated amyloid-β production in human neuron-like cells. J. Neuroinflammation *9*, 199. https://doi.org/10.1186/1742-2094-9-199.

Tcw, J., Wang, M., Pimenova, A.A., Bowles, K.R., Hartley, B.J., Lacin, E., Machlovi, S.I., Abdelaal, R., Karch, C.M., Phatnani, H., et al. (2017). An efficient platform for astrocyte differentiation from human induced pluripotent Stem cells. Stem Cell Rep. *9*, 600–614. https://doi.org/10.1016/j.stemcr.2017.06.018.

Thompson, O., Moghraby, J.S., Ayscough, K.R., and Winder, S.J. (2012). Depletion of the actin bundling protein SM22/transgelin increases actin dynamics and enhances the tumourigenic phenotypes of cells. BMC Cell Biol. *13*, 1. https://doi.org/10.1186/1471-2121-13-1.

Tilstra, J.S., Clauson, C.L., Niedernhofer, L.J., and Robbins, P.D. (2011). NF-κB in aging and disease. Aging Dis. *2*, 449–465.

Tzioras, M., Davies, C., Newman, A., Jackson, R., and Spires-Jones, T. (2019). Invited Review: APOE at the interface of inflammation, neurodegeneration and pathological protein spread in Alzheimer's disease. Neuropathol. Appl. Neurobiol. *45*, 327–346. https://doi.org/10.1111/nan.12529.

Verkhratsky, A., and Nedergaard, M. (2018). Physiology of astroglia. Physiol. Rev. *98*, 239–389. https://doi.org/10.1152/physrev.00042.2016.

Vivoli, M., Novak, H.R., Littlechild, J.A., and Harmer, N.J. (2014). Determination of protein-ligand interactions using differential scanning fluorimetry. JoVE, 51809. https://doi.org/10.3791/51809.

Wang, C., Najm, R., Xu, Q., Jeong, D.E., Walker, D., Balestra, M.E., Yoon, S.Y., Yuan, H., Li, G., Miller, Z.A., et al. (2018). Gain of toxic apolipoprotein E4 effects in human iPSC-derived neurons is ameliorated by a small-molecule structure corrector. Nat. Med. *24*, 647–657. https://doi.org/10.1038/s41591-018-0004-z.

Wang, C., Xiong, M., Gratuze, M., Bao, X., Shi, Y., Andhey, P.S., Manis, M., Schroeder, C., Yin, Z., Madore, C., et al. (2021). Selective removal of astrocytic APOE4 strongly protects against tau-mediated neurodegeneration and decreases synaptic phagocytosis by microglia. Neuron *109*, 1657–1674.e7. https://doi.org/10.1016/j.neuron.2021.03.024.

Wang, C., Fan, L., Khawaja, R.R., Liu, B., Zhan, L., Kodama, L., Chin, M., Li, Y., Le, D., Zhou, Y., et al. (2022). Microglial NF-κB drives tau spreading and toxicity in a mouse model of tauopathy. Nat. Commun. *13*, 1969. https://doi.org/10.1038/s41467-022-29552-6.

Wang, W.-Y., Tan, M.-S., Yu, J.-T., and Tan, L. (2015). Role of pro-inflammatory cytokines released from microglia in Alzheimer's disease. Ann. Transl. Med. *3*, 136. https://doi.org/10.3978/j.issn.2305-5839.2015.03.49.

Yin, C., Ackermann, S., Ma, Z., Mohanta, S.K., Zhang, C., Li, Y., Nietzsche, S., Westermann, M., Peng, L., Hu, D., et al. (2019). ApoE attenuates unresolvable inflammation by complex formation with activated C1q. Nat. Med. *25*, 496–506. https://doi.org/10.1038/s41591-018-0336-8.

Zhang, H., Wu, L.-M., and Wu, J. (2011). Cross-talk between apolipoprotein E and cytokines. Mediators Inflamm. *2011*, 949072. https://doi.org/10.1155/2011/949072.

Zhang, Y., Sloan, S.A., Clarke, L.E., Caneda, C., Plaza, C.A., Blumenthal, P.D., Vogel, H., Steinberg, G.K., Edwards, M.S.B., Li, G., et al. (2016). Purification and characterization of progenitor and mature human astrocytes reveals transcriptional and functional differences with mouse. Neuron *89*, 37–53. https://doi.org/10.1016/j.neuron.2015.11.013.

Zhou, Y., Zhou, B., Pache, L., Chang, M., Khodabakhshi, A.H., Tanaseichuk, O., Benner, C., and Chanda, S.K. (2019). Metascape provides a biologist-oriented resource for the analysis of systems-level datasets. Nat. Commun. *10*, 1523. https://doi.org/10.1038/s41467-019-09234-6.

Zhu, Y., Nwabuisi-Heath, E., Dumanis, S.B., Tai, L.M., Yu, C., Rebeck, G.W., and Ladu, M.J. (2012). APOE genotype alters glial activation and loss of synaptic markers in mice. Glia *60*, 559–569. https://doi.org/10.1002/glia.22289.

STAR★METHODS

KEY RESOURCES TABLE

REAGENT or RESOURCE	SOURCE	IDENTIFIER
Antibodies		
Anti-APOE4 (4E4)	Enzo Life	Cat#ENZ-ABS295-0100
Anti-APOE pan (F-9)	Santa Cruz	Cat#sc-390925; AB_2892618
Anti-IL-6	Santa Cruz	Cat#sc-130326; RRID:AB_2127744
Anti-IL-8	Santa Cruz	Cat#sc-376750; RRID:AB_2891256
Anti-IκBα (44D4)	Cell Signaling	Cat#4812S
Anti-Phospho-IκBα (Ser32) (14D4)	Cell Signaling	Cat#2859S
Anti-NFκB p50 (H-119)	Santa Cruz	Cat#sc-7178; RRID:AB_650211
Anti-NFκp52 (05-361)	Millipore	Cat#05-361; RRID: AB_309692
Anti-NFκp65 (F-6)	Santa Cruz	Cat#sc-8008; RRID:AB_628017
Anti-Phospho-NFκp65 (S536)	Cell Signaling	Cat#3031S
Anti-Actin	Sigma-Aldrich	Cat#A5316; RRID:AB_476743
Anti-GAPDH	Sigma-Aldrich	Cat#G8795; RRID:AB_1078991
Anti-Histone 3	Cell Signaling	Cat#9715; RRID:AB_331563
Anti-NANOG	Abcam	Cat#ab21624; RRID: AB_446437
Anti-Vimentin	Cell Signaling	Cat#3932S
Anti-GLAST	Thermofisher	Cat#PA5-34198; RRID: AB_2551551
Anti-ALDH1L1	Abcam	Cat#ab190298; RRID: AB_2857848
Goat-anti Mouse IgG (H+L) Secondary Antibody, HRP	Thermofisher	Cat# G-21040, RRID:AB_2536527
Goat-anti Rabbit IgG (H+L) Secondary Antibody, HRP	Thermofisher	Cat# G-21234, RRID:AB_2536530
Bacterial and virus strains		
Subcloning Efficiency™ DH5α Competent Cells	Invitrogen	Cat#18265017
Biological samples		
Human post-mortem brain tissues (AD), Table S4.	Neuro-CEB brain bank	N/A
Chemicals, peptides, and recombinant proteins		
Phalloïdin	Thermofisher	Cat#A30107
Hoechst	sigma-Aldrich	Cat#33342
Recombinant human ApoE3	Peprotech	Cat#350-02
Recombinant human ApoE4	Peprotech	Cat#350-04
PH-002	Calbiochem, Sigma Aldrich	Cat#178477
Recombinant human TAGLN3	Abcam	Cat#ab116179
Vorinostat (SAHA)	Sigma-Aldrich	Cat#SML0061
Recombinant human TNF-a	Peprotech	Cat#300-01A
Recombinant human IL-1b	Peprotech	Cat#200-01B
Recombinant human MCP-1	Peprotech	Cat#300-04
growth-factor-reduced Matrigel	Corning	Cat#354230
EDTA	Gibco- Thermofisher	Cat#R1021
DPBS no calcium no magnesium	Gibco- Thermofisher	Cat#14190144
STEMdiff™ SMADi Neural Induction Kit	Stem cell technologies	Cat#05835
StemPro™ Accutase	Gibco- Thermofisher	Cat#A11105

(*Continued on next page*)

Continued

REAGENT or RESOURCE	SOURCE	IDENTIFIER
Dulbecco's Modified Eagle Medium (DMEM)/F12	Gibco- Thermofisher	Cat# 10565018
KnockOut™ Serum Replacement	Gibco- Thermofisher	Cat#A3181501
Y-27632	Tocris Bioscience	Cat#1254
STEMdiff™ Neural Progenitor Medium	Stem cell technologies	Cat#05833
Astrocyte medium+FBS+AGS+P/S supplement	ScienceCell	Cat#1801; Cat#0010; Cat#1852; Cat#0503
StemMACS™ iPS-Brew XF medium, human	Miltenyi	Cat#130-104-368
PrimeSTAR GXL Kit	Clontech, Takara Bio Europe	Cat#R050B
Proteinase K	Roche Diagnostics	Cat#03115887001
AMPureXP	Beckman Coulter	Cat#A63882
RIPA buffer	Sigma-Aldrich	Cat#R0278
Protease inhibitors	Millipore	Cat#539132
Protease/Phosphatase Inhibitor Cocktail	Cell Signaling	Cat#5872
Bio-Rad DC™ protein assay kit	Biorad	Cat##5000111
TRIzol™ Reagent	Thermofisher	Cat#15596026
Antigenfix	Diapath	Cat#P0016
Amersham ECL Prime	GE Healthcare	Cat# RPN2232
Critical commercial assays		
Human IL-8 Standard ABTS ELISA Development Kit	Peprotech	Cat#900-K18
Human IL-6 Standard ABTS ELISA Development Kit	Peprotech	Cat#900-K16
High-Capacity RNA-to-cDNA™ Kit	Thermofisher	Cat#4388950
NucleoSpin® Plasmid kit	Macherey Nagel	Cat#740588.50
NucleoBond® Xtra Midi EF kit	Macherey Nagel	Cat#12773550
Neon™ Transfection System	Invitrogen	Cat#10124334
Human Gene Expression microarray slides (8×60K v2 Microarray Kit)	Agilent technologies	Cat#G4851B
NucleoSpin™ RNA Plus	Macherey Nagel	Cat#740984.50
iTaq Universal SYBR Green Supermix	Bio-Rad Laboratories	Cat#172-5121
ProteoExtract® Subcellular Proteome Extraction Kit	Calbiochem	Cat#539790
Deposited data		
DNA microarray	ArrayExpress database	E-MTAB-9625 www.ebi.ac.uk/arrayexpress
Experimental models: Cell lines		
hiPSC lines (Table S1)	Coriell Institute for Medical Research	From NIGMS Human Genetic Cell Repository/ CIRM iPSC Repository
Oligonucleotides		
See Table S5 for oligonucleotides used for CRISPR-Cas9 experiments	This paper	N/A
See Table S6 for APOE genotyping primers	This paper	N/A
See Table S7 for qPCR primers	This paper	N/A
Recombinant DNA		
pSpCas9 (BB)-2A-Puro (PX459) V2.0	Addgene	Cat#62988
pSpCas9 (BB)-2A-Puro (PX459) V2.0 with EF1 alpha promoter	This paper	N/A

(*Continued on next page*)

Continued		
REAGENT or RESOURCE	SOURCE	IDENTIFIER
Software and algorithms		
Metascape	Metascape	https://metascape.org
Fiji	ImageJ	https://fiji.sc/
Prism8	GraphPad	https://www.graphpad.com/scientific-software/prism/
Zen software	Zeiss	N/A
Other		
Zeiss LSM 710 Laser Scanning Confocal Microscope	Zeiss	LSM710
Axio-Observer upright epifluorescence microscope	Zeiss	N/A
Essential V6 imaging platform	Uvitec	N/A
NanoDrop™-1000 Spectrophotometer	Thermo Fisher Scientific	N/A
7500 Fast Real-Time PCR System	Thermo Fisher Scientific	N/A

RESOURCE AVAILABILITY

Lead contact

Further information and requests for resources and reagents should be directed to and will be fulfilled by the Lead Contact, Emmanuel Nivet (emmanuel.nivet@univ-amu.fr).

Material availability

- Plasmids generated in this study are available from the lead contact with a completed Materials Transfer Agreement.
- Any additional There are restrictions to the availability of original cell lines and their genome-edited version due to a Materials Transfer Agreement that prohibits secondary distribution. However, the lead contact will take proper action to make the material available on a request-basis, when permitted.

Data and code availability

- DNA microarray data have been deposited to the ArrayExpress database and are available to the public as of data of publication. The accession number is listed in the key resources table.
- This paper does not report any original code.
- Any additional information required to reanalyze the data reported in this paper is available from the lead contact upon request.

EXPERIMENTAL MODEL AND SUBJECT DETAILS

Human iPS cells (hiPSC)

All hiPSC lines used in this study were purchased from the Coriell biorepository. The following cell line was obtained from the NIGMS Human Genetic Cell Repository at the Coriell Institute for Medical Research [GM24666]. The following cell lines were obtained from the CIRM iPSC Repository at the Coriell Institute for Medical Research [CW70019, CW50028, CW50052, CW50069, CW50082]. Information about hiPSC lines are indicated in Table S1 and a certificate of analysis for each of these lines is available from suppliers. In this study, patient/donor -specific hiPSCs carrying the same APOE genotype were considered as biological replicates. All hiPSC lines used in this study were obtained with approved MTAs from the Aix-Marseille University thus complying with all relevant ethical regulations.

Human *post-mortem* brain tissues

Post-mortem human cortical brain tissue samples (temporal lobe) from 10 patients diagnosed for sAD and 6 control patients not diagnosed for AD were obtained from Neuro-CEB brain bank of Hôpital de la Pitié-Salpétrière (Paris, France) after informed consent of all participants during their life and/or their legal guardians. Characteristics of the population of patients such as *APOE* genotype, sex, age, post-mortem delay of storage and Braak stage are scoring by members of the Neuro-Ceb and listed in Table S4. All tissues were obtained following informed consent, flash frozen at time of autopsy indicated in Table S4 and stored at −80°C until being processed for analyses. All brain samples used in this study were obtained with approved MTAs from the Aix-Marseille University thus complying with all relevant ethical regulations.

METHOD DETAILS

Culture of human iPSC (hiPSC) lines

hiPSCs were cultured and maintained undifferentiated in a chemically defined growth media (StemMACS^{TM} iPS-Brew XF medium; Miltenyi Biotec, Paris, France) onto growth-factor-reduced Matrigel^{TM} (Corning)-coated plates (8,6μg/cm^2). In short, when reaching 70–80% confluency, hiPSCs were treated with an enzyme-free solution (hereafter referred as Gentle Dissociation Solution) containing 0.5 mM EDTA (Gibco, Thermofisher, Waltham, Massachusetts, USA), DPBS without Ca^{2+} and Mg^{2+} (Gibco) and 1.8 mg/mL NaCl (Sigma-Aldrich, Saint-Louis, Missouri, USA). hiPSCs were incubated for 2 min in Gentle Dissociation Solution at Room Temperature (RT). The colonies were then broken into small clusters and lifted carefully using a 5 mL glass pipette at a ratio of 1:4. When necessary, differentiated areas were removed from hiPSC cultures prior to passaging in order to maintain the cultures undifferentiated before proceeding to their differentiation. hiPSC lines were maintained in an incubator (37°C, 5% CO_2) with medium changes every day.

Differentiation of neural progenitors cells (NPCs) from hiPSCs

Human iPSCs were differentiated into neural progenitor cells (NPCs) following a monolayer culture method with a commercial dual SMAD inhibition-mediated neural induction medium (STEMdiff^{TM} SMADi Neural Induction Kit, Stem Cell Technologies, Vancouver, Canada) based on a published protocol (Chambers et al., 2009). NPCs were obtained following manufacturer's instructions with slight modifications. Undifferentiated cultures of hiPSCs were treated with Gentle Dissociation Solution for 4 min, then the solution was removed, and cells were incubated in StemPro^{TM} Accutase^{TM} (Gibco) for 4 min. hiPSCs were then dislodged as single cell and transferred into Dulbecco's Modified Eagle Medium (DMEM)/F12 (Gibco) supplemented with 20% KnockOut^{TM} Serum Replacement (Gibco). Then, cells were centrifuged at 200 x g for 5 min, resuspended in DPBS without Ca^{2+} and Mg2+, counted and centrifuged once more at 200 x g for 5 min. Last, cells were resuspended in STEMdiff^{TM} SMADi Neural Induction Kit + 10 μM Y-27632 (Tocris Bioscience, Bristol, UK), a Rho-associated protein kinase inhibitor, plated onto growth-factor-reduced Matrigel^{TM}-coated plates (8.6μg/cm2) (320,000 cells/cm2) and maintained in an incubator (37°C, 5% CO2) with medium changes every day. Between 6 and 9 days after induction, cells were harvested as single cell using Accutase^{TM}, transferred into DMEM/F12 media, centrifuged at 200 x g for 5 min, resuspended in STEMdiff^{TM} SMADi medium + 10 μM Y-27632, plated onto growth-factor-reduced Matrigel^{TM}--coated plates (270,000 cells/cm2) and maintained in an incubator (37°C, 5% CO2) with medium changes every day for 5 additional days. Then, cells were passaged one more time following the same procedure. Five days after the last passage (i.e., between 16 to 19 days post-induction), differentiated cells were harvested as single cells using Accutase^{TM}, centrifuged at 200 x g for 5 min prior to be resuspended in STEMdiff^{TM} Neural Progenitor Medium (Stem Cell Technologies) and seeded onto growth-factor-reduced Matrigel^{TM}-coated plates (8.6μg/cm2) at 125,000 cells/cm2. Cells were maintained in an incubator (37°C, 5% CO2) with medium changes every day and passaged with Accutase^{TM} when reaching 80–90% confluency. Of note, hiPSC-NPCs between passage 2 and 5 were used for further maturation into astrocytes.

Differentiation of astrocytes-like cells from NPCs

hiPSCs-derived NPCs were differentiated into astrocytes according to a previous protocol (Tcw et al., 2017). In short, NPCs were dissociated as single cell with Accutase^{TM} and seeded at 30,000 cells/cm^2 on growth-factor-reduced Matrigel^{TM}-coated plates (8.6μg/cm^2) in astrocyte medium (ScienCell, Carlsbad, California, USA). Full medium changes were performed every 72 hours over a 30 day-differentiation period. When cells reached 90–95% confluency (approximately 5–7 days after initial seeding), they were passaged as single cell into astrocyte medium and cultured onto growth-factor-reduced Matrigel^{TM}-coated plates (8.6μg/cm^2) at 30,000 cells/cm^2. For passaging, hiPSC-astrocytes were washed with DPBS without Ca^{2+} and Mg^{2+}, incubated 5 min with Accutase^{TM}, dissociated, washed with DMEM/F12 prior to be centrifugated at 200 x *g* for 5 min and resuspended with astrocyte medium. From the next passage, differentiated astrocytes were passaged at a 1:3 ratio on a weekly basis and expanded in astrocyte medium. Astrocytes between 35 and 45 days of differentiation were used throughout the study. Cells ongoing astrocyte differentiation were maintained in an incubator (37°C, 5% CO_2) with medium changes twice a week. Of note, in this study, for a given APOE genotype, each independent iPSC line is a biological replicate and each batch of astrocytic differentiation from a given iPSC line - i.e. astrocytes generated from independent differentiation onsets - is a technical replicate.

CRISPR/Cas9 gene correction

To enable deeper analysis of APOE4 effects on inflammation in human astrocytes, we used CRISPR/Cas9 gene editing to generate [*APOE4/E4*]-Ki and APOE-KO isogenic clones (3 independent clones for each) from two different parental lines: a parental [*APOE3/E3*] line derived from a ND control donor (ND-1) and a parental [*APOE3/E3*] line derived from a sAD patient (sAD-4) (Table S1).

Preparation of the CRISPR/Cas9-ApoE sgRNA plasmid

A CRISPR/Cas9-APOE sgRNA plasmid was prepared following a published protocol (Ran et al., 2013). Briefly, we designed a sgRNA sequence within 20 nucleotides from the target site (exon 4, amino acid 112) selected with the Bioinformatic tool CRISPOR (crispor.tefor.net). This sgRNA was chosen specifically to guide the Cas9 to cleave the double strand of DNA 3 base pairs upstream of a PAM sequence that is near to the gene region responsible for the APOE4 polymorphism. The same sgRNA was used to generate [*APOE4/E4*]-Ki and APOE-KO isogenic clones. The sgRNA sequence was as follows (5'>3''): GCGGACATGGAGGACGTGTG (see also Table S5).

We used pSpCas9 (BB)-2A-Puro (PX459) V2.0 (Addgene plasmid # 62988, Addgene, Teddington, UK) and modified it to replace the CMV promoter by the EF1 alpha promoter. The human EF1 alpha promoter was amplified from hiPSCs with the primers pAB01 and pAB02 (5′-aattctgcagacaaatggctctagaGGCTCCGGTGCCCGTCAGTG-3′ and 5′-tccttatagtccatggtggcaccggTCACGACACCT GAAATGGAAG-3′), respectively (see also Table S5). The final product cAB03 (*i.e.*, pX459-pEF1alpha) was then obtained by SLIC method mixing the pX459 fragment and the EF1alpha PCR product as previously described (Jeong et al., 2012).

The sgRNA was cloned into the cAB03 open plasmid vector. For cloning, oligonucleotide pairs were hybridized with a buffer containing Tris HCl (100 mM) and NaCl (500 mM) and placed in a thermocycler ramping from 95°C to 18°C at 0.05°C/s. cAB03 was opened with BbsI (New England Labs Inc., Ipswich, Massachusetts, USA), then ligated with annealed oligonucleotides by incubating with T4 DNA Ligase (New England Labs Inc.) 10 min at RT. The ligation product was transformed in competent bacteria DH5α (Invitrogen, Waltham, Massachusetts, USA) following manufacturer's instructions. After incubation for 1 h at 37°C, the bacteria were inoculated onto ampicillin-containing LB agar plates (100 μg/mL) and incubated overnight at 37°C. The next day, half of the bacterial colony was replated onto an ampicillin LB agar plate and the other half was extracted 10 min at 95°C in a lysis buffer containing 20 mM Tris HCl, 2 mM EDTA and 1% Triton 100X (pH 8). Then, a PCR was performed to verify guide insertion, using primer Pr1127 (5′-AC TATCATATGCTTACCGTAAC-3′, see also Table S5) that binds to the backbone and the reverse oligonucleotide used to insert the sgRNA. The PCR product was put to migrate on a 2% gel to verify the insertion of the sgRNA (100 bp band) in the bacteria. One or two positive clones were then sent for sequencing to confirm the presence of the sgRNA in the plasmid after miniprep extraction (NucleoSpin® Plasmid kit, Macherey Nagel, Allentown, Pennsylvania, USA). A validated clone was then amplified, its DNA extracted by midiprep (NucleoBond® Xtra Midi EF kit, Macherey), assayed and stored at −20°C.

Single-stranded OligodeoxyNucleotide (ssODN) design

We also designed single-stranded oligodeoxynucleotides (ssODN) to convert *APOE3* to *APOE4* with an editing site closed to the PAM in order to prevent recurrent Cas9 cutting in edited cells. The sequence of the donor DNA (127 nucleotides) has been chosen so that it contains the polymorphism site responsible for the *APOE4* status (bold): GCGGACATGGAGGACGTGCG. Arms of homology have been added on either side of this sequence to be complementary to the target region. The ssODN sequence was as follows (5'>3''): CCT GCA CCT CGC CGC GGT ACT GCA CCA GGC GGC CGC GCA CGT CCT CCA TGT CCG CGC CCA GCC GGG CCT GCG CCG CCT GCA GCT CCT TGG ACA GCC GTG CCC GCG TCT CCT CCG CCA CCG GGG TCA G. This ssODN sequence is also listed in Table S5.

Electroporation

Undifferentiated hiPSCs were treated with Gentle Dissociation Solution for 4 min at RT. The Gentle Dissociation Solution was then removed, and cells were treated with Accutase™ for 4 additional minutes at 37°C. Cells were collected as single cells (*i.e.*, dissociated colonies) and transferred into a tube containing a solution of DMEM/F12 supplemented with 20% of Knock-Out Serum Replacement, using a minimum of 5 times the volume of Accutase™ used for cell dissociation. Cells were centrifuged at 200 x g for 5 min, the cell pellet was washed with DPBS without Ca^{2+} and Mg^{2+}. Cells were centrifuged one more time at 200 x g for 5 min. The cell pellet was then re-suspended with the Resuspension Buffer R (Neon™ Transfection System 100 μL Kit, Invitrogen) to a final concentration of 10,000 cells/μL. 100 μL of the cell suspension were transferred to a sterile 1.5 mL microcentrifuge tube and mixed with 4 μg of sgRNA (generation of KO) or 4 μg of sgRNA along with 4 μg of ssODN (1:1 ratio). Cells were then electroporated with the Neon™ Transfection System using the following parameters: 1,100V, 30 ms, 1 pulse. The electroporated cell suspension was then flushed into 1 well of a 6-well Matrigel-coated plate containing StemMACS™ iPS-Brew XF medium supplemented with 10 μM of Y-27632. Of note, one well containing cells electroporated without plasmids was used as control to define the best time window at which the puromycin treatment had to be stopped to select the electroporated cells. The next day, media was replaced with StemMACS™ iPS-Brew XF medium supplemented with puromycin (1μg/μL) until all control electroprated cells died. Puromycin-resistant cells were maintained in culture with iPS-Brew medium and changed every second day until clonal colonies could be observed.

Clone isolation and screening

Each individual colony (*i.e.*, those arising from a single/isolated cell after antibiotic selection) was manually picked under a microscope and cut in two halves: one half was used for genomic DNA extraction followed by PCR screening and the other half was slightly dissociated by 2–3 up and down pipetting (using a 200 μL pipette tip) and plated back onto one well of a 24-well Matrigel-coated plate containing StemMACS™ iPS-Brew XF medium supplemented with 10 μM of Y-27632. Regarding the latter, each clone was maintained in culture until (in)-validation for the KO or Ki of interest as evaluated by PCR analysis.

For genomic DNA extraction, one half of each of the puro resistant/picked colonies was individually transferred into a 0.2 mL PCR tube and centrifuged 5 min at 300 x g. The supernatant was then removed, and the pellet washed with 150 μL DPBS without Ca^{2+} and Mg^{2+} and centrifuged 5 min at 300 x g. The supernatant was removed and the cell pellet re-suspended with a 20 μL mix containing: 1X of the 5X PrimeSTAR GXL Buffer (Clontech, Takara Bio, Shiga, Japan), proteinase K (0.167 mg/mL, Roche Diagnostics, Basel, Switzerland) and ddH_2O. DNA extraction was performed using a thermocycler with the following settings: 3 h at 55°C and 30 min at 95°C. Then, a 20 μL PCR reaction was performed using 5 μL of the extracted genomic DNA and 15 μL of a PCR mix containing 1X of the 5X PrimeSTAR GXL Buffer, PrimeSTAR GXL DNA polymerase (0.25 U/10 μL), dNTPs (200 μM each) and the specific primers for each genotypic situation reported in Table S6; and PCR reaction was performed using the following PCR conditions: 1 min at 94°C for one cycle, then 10 sec at 98°C, 30 sec at 65°C, 45 sec at 68°C for 35 cycles and to finish, 5 min at 68°C for one cycle.

In the case of the screening of the KO clones, the PCR product was digested with the AflII enzyme (New England Biolabs, NEB, Ipswich, Massachusetts, USA) whose recognition site is at the targeted cut-off site. Thus, if a clone was KO, the enzyme was not able

to cut the DNA. In the case of KI clones, PCR screening was performed by dCAPS method(Neff et al., 1998) so that the PCR product includes a recognition site for BssHII if and only if the expected gene editing is effective. The PCR products from each clone were then digested by BssHII, and the samples were deposited to migrate onto a 3% agarose gel and revealed to analyze the size of the amplicon for each individual clone.

Expected profiles:.
- APOE-KO: screening with pEN23 and pEN24 primers (digestion with AflIII)
  - For APOE- KO clones: 2 bands at 576 bp and 156 bp
  - For WT clones: 1 band at 700 bp
- [*APOE4/E4*]-Ki: screening with APOE03 and APOE04 primers (digestion with BssHII)
  - For edition into APOE4 homozygous: 2 bands at 101 bp and 51 bp
  - For WT clones (APOE3): 1 band at 152 bp

The DNA of clones identified as possibly KO or Ki was purified using magnetic beads (AMPureXP, Beckman Coulter, Brea, California, USA) and the samples were sequenced by the Sanger method. Analyses of Sanger traces were done using Snapgene software. Briefly, sequences of KO or Ki PCR-based pre-selected clones were aligned with WT sequence to ultimately confirm the successful edition to generate KO or Ki isogenic clones. Positives clones were kept, amplified and confirmed again by Western blot analyses prior amplification for further experiments. A minimum of 3 independent clones for each of the edited hiPSC lines were produced to test inter-clone reproducibility of the results and so exclude biased results due to putative off-targets effects in a given clone.

Karyotyping

Karyotyping was performed on actively dividing iPSCs, using standard RHG-banding protocols, in the Chromostem platform of the University Hospital of Montpellier. After metaphase arrest induced by Colcemid, the cells were hypotonically shocked in 0.075 M KCL solution, fixed with methanol/acetic acid solution (3/1) and then dropped onto clean slides. At least 20 metaphases were analyzed for each cell lines using a conventional microscope and Ikaros software (Metasystems, Altlussheim, Germany).

Astrocytes treatment

For each experiment/condition involving a specific treatment (as described below), a nearly confluent culture of hiPSC-derived astrocytes was passaged at a 1:3 ratio and treatment was applied when the cell reached a 70% confluence (30–45 days of differentiation).

Pro-inflammatory cocktail

Astrocytes were treated with a defined cocktail of pro-inflammatory mediators composed by three human recombinant proteins TNF-α, MCP-1 and IL-1β with a concentration of 10 ng/mL each for 24 hours. Each of the three proteins were purchased from Peprotech and prepared according to the manufacturer's instructions. All three proteins were resuspended in water and so water was used as vehicle for control condition of this treatment.

APOE rescue experiments

For APOE rescue experiments, control [*APOE3/E3*] astrocytes or isogenic [*APOE4/E4*]-Ki clones were incubated for 24 hours with the pro-inflammatory cocktail and different doses (0, 15, 30, 50, 100 and 120 μg/mL) of APOE4 or APOE3, respectively, as human recombinant proteins (Peprotech, Rocky Hill, New Jersey, USA). APOE3 was resuspended in 20 mM Sodium Phosphate, pH 7.8; 0.5 mM DTT and APOE4 was resuspended in water.

[APOE3/E3] conditioned media experiments

For astrocyte conditioned media experiments, control [*APOE3/E3*] astrocytes were maintained in culture for either 72h or 168h without media changes. Of note the initial seeding density was calculated to have a nearly confluent culture at the time of collection. Freshly collected medium was then applied on PBS-washed [*APOE4/E4*]-Ki astrocyte cultures and co-treated with the pro-inflammatory cocktail for 24h.

APOE4-structure corrector

To investigate the impact of APOE4-associated structural changes on inflammation, we incubated [*APOE4/E4*]-Ki astrocytes with 100 μM of a small molecule structure corrector for APOE4 named PH-002 (Chen et al., 2012) (Calbiochem, Sigma-Aldrich) during 24 hours, followed by a full medium change containing the pro-inflammatory cocktail plus a new fresh dose of PH-002 for additional 24 hours. PH-002 was resuspended in DMSO and so DMSO was used as vehicle for control condition of this treatment.

TAGLN3 rescue experiments

To confirm the impact of TAGLN3 on the inflammatory modulation, [*APOE4/E4*]-Ki astrocytes were incubated for 24 hours with the pro-inflammatory cocktail and different doses (0.5 and 20 μg/mL) of TAGLN3 as human recombinant protein (Abcam, Cambridge, UK) prior to be analysed. TAGLN3 was resuspended 0.02% DTT, 0.32% Tris HCl, 20% Glycerol, pH 8. The same buffer was used as vehicle for control condition of this treatment.

HDAC inhibition experiments

In order to study the impact of HDAC inhibition on inflammation, we incubated astrocytes with the pro-inflammatory cocktail and 10 μM of SAHA (Vorinostat, Sigma-Aldrich) as a pan-histone deacetylase (HDAC) inhibitor. SAHA was resuspended in DMSO and so DMSO was used as vehicle for control condition of this treatment.

DNA microarray

Samples description

For DNA microarray analyses, hiPSC-derived astrocytes obtained from the differentiation of the hiPSC ND control line (CW70019), which carries the [*APOE3/E3*] genotype, were used as control. From this hiPSC line, CRISPR-Cas9-based knock-In (KI) experiments were performed to generate three independent clones (Clones #1, #2 and #3) carrying the [*APOE4/E4*] polymorphism as aforementioned. From each of these clones, independent cultures of hiPSC-derived astrocyte-like cells were generated, leading to three replicates for the [*APOE4/E4*] genotype with a technical unicate for each clone. Considering the robustness and reproducibility of our model, a technical unicate of the isogenic control line was used for microarray experiments. Each hiPSC-derived astrocyte cultures were either treated for 24 h with the pro-inflammatory cocktail (described above) prior to harvesting the samples or placed in control untreated conditions. Noteworthy, for those differentially expressed genes (APOE3/3 *versus* APOE4/4) we found of interest for this study, we performed qPCR validations by using technical replicates from each biological replicate.

Samples preparation

The samples were selected for microarray analyses provided that they had an >8.0 RNA integrity number, a clear gel image and no DNA contamination as shown by the histogram. Sample amplification, labelling, and hybridization essentially followed the one-colour microarray-based gene expression analysis (low input quick amp labelling) protocol (version 6.5, May 2010) recommended by Agilent Technologies (Santa Clara, California, USA). Then, 200 ng of each total RNA sample was reverse transcribed into cDNAs using the oligo dT-T7 promoter primer. Labelled cRNAs were synthesized from the cDNAs. The reaction was performed in a solution containing a dNTPs mix, cyanine 3-dCTP, and T7 RNA Polymerase and was incubated at 40°C for 2 h. RNeasy mini spin columns from Qiagen (Hilden, Germany) were used to purify the amplified cRNA samples. The cRNAs were quantified using a NanoDrop™ Spectrophotometer version 3.2.1 (Thermo Fisher Scientific). Six hundred nanograms of cyanine 3-labelled, linearly amplified cRNAs were used for hybridization. Hybridization on Human Gene Expression microarray slides (8×60K v2 Microarray Kit (3 slides) G4858A-039494 G3, Agilent Technologies) containing 60,000 oligonucleotide probes was performed in a 65°C hybridization oven for 17 h at 10 rpm. The hybridized microarray slides were then washed according to the manufacturer's instructions and scanned using an Agilent Microarray Scanner with the Agilent Feature Extraction Software (Agilent Technologies). AgiND R package was used for quality control and normalization. Quantile methods and a background correction were applied for data normalization. Microarray data are available in the ArrayExpress database (164. ArrayExpress database. [www.ebi.ac.uk/arrayexpress]) under accession number E-MTAB-9625.

Data analysis

Only genes whose intensity values were different from background were considered. Genes were selected according to a fold change superior or equal to 1.5 for those upregulated and inferior or equal to 0.6 for those downregulated. Biological interpretation of the data was performed using the Java/Perl software Predictsearch® (Laboratoire Genex [www.laboratoire-genex.fr]), which has been previously described (Patatian and Benech, 2020). PredictSearch® is a powerful text mining software that identifies correlations between genes and biological processes/diseases within all scientific publications, cited at least one gene or one of its aliases in the PubMed database. The relevance of the functional correlations is supported by the Fisher test, which allows the statistical analysis of co-citations. PredictSearch® software characterizes the pathways and functional networks in which the selected genes found to be modulated are involved. Pathway analysis was performed using metascape (https://metascape.org)(Zhou et al., 2019).

Total RNA isolation and quantitative real-time PCR analysis for mRNA expression

The total RNA was extracted from cultured cells with NucleoSpin™ RNA Plus (Macherey-Nagel), according to the manufacturer's recommendations. RNA concentration and purity were determined using a NanoDrop™-1000 Spectrophotometer (Thermo Fisher Scientific). Single-stranded cDNA were synthesized from 500 ng of RNA using High-Capacity RNA to cDNA™ kit (Thermo Fisher Scientific) suitable for quantitative PCR. RT-qPCR experiments were performed with the 7500 Fast Real-Time PCR System (Applied Biosystems/Life Technologies). All reactions were performed using primers ordered from Integrated DNA Technologies (IDT) as 25 nmole DNA oligos and resuspended following manufacturer's recommendations; and the iTaq Universal SYBR Green Supermix (Bio-Rad Laboratories, Hercules, California, USA). Relative expression levels were determined according to the ΔΔCt method with the human housekeeping *ACTIN* gene as endogenous control for normalization. For each condition, RNA extractions were performed from independent cultures and the reported values are the mean fold change relative to the value of the control sample (untreated cell line or isogenic control line, depending of the experiment). Primer sequences are listed in Table S7.

Sub-cellular fractionation

Cytoplasmic and nuclear fractions were prepared from cell lysates using a ProteoExtract® Subcellular Proteome Extraction Kit (Calbiochem, San Diego, California, USA) according to the manufacturer's instructions. The purity of each fraction was analyzed by immunoblotting using antibodies against Histone 3 and GAPDH for nuclear and cytoplasmic fractions, respectively.

Immunoblotting and protein quantification

Supernatants from cells were collected and stored at −80°C in Protein LoBind Tube (Eppendorf). Cell lysates were scraped in RIPA buffer (Sigma-Aldrich) containing a cocktail of protease inhibitors (Millipore, Burlington, Massachusetts, USA) or Protease/

Phosphatase Inhibitor Cocktail (Cell Signaling, Danvers, Massachusetts, USA) and sonicated. For each sample, the protein concentration was determined using a Bio-Rad DC™ protein assay kit (Bio-Rad). Proteins (15 μg) were loaded onto precasted Tris-Tricine 16% low molecular weight gels or pre-casted Tris-Glycine 4–20% gels (Thermo Fisher Scientific) and transferred onto nitrocellulose membranes (GE Healthcare, Chicago, Illinois, USA). After blocking with 5% milk in PBS 1X, 0.2% Tween 20 (Sigma Aldrich) (or TBS for optimized protocol for detection of phospho-proteins), membranes were probed with primary antibodies against the protein of interest. Then, the appropriate HRP-conjugated secondary IgG antibodies were used (LifeTechnologies, Carlsbad, California, USA) at an appropriate dilution based on primary antibody dilution. Immunoblot signals were visualized with Essential V6 imaging platform (UVITEC, Cambridge, UK) using the Amersham ECL Prime (GE Healthcare) and quantified using ImageJ software. Briefly, the expression of a given protein of interest was normalized with ACTIN for cell lysate immunoblots and with Ponceau staining for supernatant immunoblots. The list of antibodies used in this study is reported in the key resources table.

ELISA procedure

The levels of IL-6 and IL-8 from astrocyte culture supernatants were determined using the human IL-6 and IL-8 ELISA Development Kit respectively (Peprotech, Neuilly-sur-Seine, France) according to the manufacturer's recommendations.

Differential scanning fluorimetry (DSF)

Thermal stability of TAGLN3 in the presence of different concentrations of NFκBα were measured in 50 mM Tris-HCl, 1 mM TCEP, buffer at pH 7.5 using nano differential scanning fluorimetry (DSF) instrument Prometheus NT.Plex (NanoTemper Technologies, München, Germany). NanoDSF grade capillaries were filled with 5 μM TAGLN3 solution. Concentrations of IκBα varied from 0 to 30 μM. The capillaries were loaded into the Prometheus NT.Plex instrument and the ratio of TAGLN3 fluorescence emission intensities at 330 nm (I330) and 350 nm (I350) was registered upon capillaries heating from 15°C to 95°C at rate of 1 K/min. The unfolding mid-transition temperature (T_m) was determined from first derivative of the temperature dependence of the ratio, as implemented in Prometheus NT.Plex software. The dependence of TAGLN3 T_m from IκBα concentration was plotted and fitted using 1:1 binding model as described before(Vivoli et al., 2014) to estimate dissociation constant (K_d).

Human brain tissues analysis

Sample preparation

For protein extraction, brain tissue samples of 100 ± 5 mg were lysed in 1 mL of RIPA containing a cocktail of protease inhibitors (Millipore), homogenized with Dounce homogenizer (Dutcher, Bernolshneim, France), tubes were agitated 10 min at 4°C and centrifugated at 12,000 x *g* for 10 min at 4°C. Then, the supernatants were transferred into a new set of tubes and protein concentration was determined using Bio-Rad DC™ protein assay kit (Bio-Rad). Western blot protocol is the same as described before. Note that 30 μg of total protein was loaded in this case.

For RNA extraction, 80 ± 5 mg of brain tissue samples were lysed in 1 mL of TRIzol™ Reagent (Thermo Fisher), according to the manufacturer's recommendations. RT-qPCR protocol is the same as described before.

Immunofluorescence labelling experiments

Cells were fixed in 4% paraformaldehyde (Antigenfix, Diapath, Martinengo, Italia) for 10 minutes at RT before immunostaining. After blocking with PBS 1X, 3% BSA, 0.1% Triton, cells were incubated overnight at 4°C with the following primary antibodies: NANOG, ALDH1L1, Vimentin and GLAST. The corresponding secondary antibodies (coupled to Alexa Fluor® 488 or 568, LifeTechnologies, 1:800) and Hoechst (Sigma-Aldrich, 1/800) for 2 hours at RT. The list of antibodies used in this study is reported in the key resources table. Cells were examined using a Zeiss LSM 710 Laser Scanning Confocal Microscope (Zeiss, Oberkochen, Germany) or an Axio-Observer upright epifluorescence microscope (Zeiss) and post-acquisition was performed using the Zen software (Zeiss) and/or the Fiji (ImageJ) software.

QUANTIFICATION AND STATISTICAL ANALYSIS

Sample size was chosen to ensure sufficient statistical power for each assay throughout the study. All statistical analyses were performed using GraphPad Prism software on mean values calculated from the averages of biological and/or technical replicates. In all assays, we used multiple and independent batches of differentiation from each of the tested lines/clones, adding further statistical power. Thus, on the figures, the individual dots in the bar charts represent independent differentiation onset. In short, hiPSC lines derived from ND and sAD patients (ND-1, ND-2, sAD-1, sAD-2, sAD-3 and sAD-4) were differentiated in astrocyte-like cells with 3 to 7 independent batches for analyses as replicates. For isogenic Ki and KO clones from both ND-1 and sAD-4, 3 independent clones were generated and differentiated into astrocyte-like cells with 3 to 8 independent batches for analyses as replicates. For each line, 3 independent clones were generated to: i) avoid biased results due to off-target effect, as the chance to get the same off-target modification in 3 independent clones are statistically extremely low; ii) offer the possibility to repeat experiments in three different clones, providing enough statistical power.

Statistical significance was calculated by two-tailed unpaired Student's t-test to compare two experimental groups or one-way ANOVA (multicomparisons, three or more conditions) followed by Dunnett's post-hoc test or by Fisher's least significant difference (LSD) test for differences of means between each group and the control group of data or followed by Tukey's post-hoc test for multiple comparison between groups, with $p < 0.05$ considered statistically significant. The exact p values are always reported, except when $p < 0.0001$. No values were excluded from the analyses. Sample sizes for all experiments were chosen based on previous experiences. Independent experiments were pooled and analysed together whenever possible as detailed in figure legends. All graphs show mean values ± SEM.